A MATHEMATICAL MODEL TO PREDICT δ-FERRITE CONTENT IN AUSTENITIC STAINLESS STEEL WELD METALS

M.A. Valiente Bermejo

Dr. María Asunción VALIENTE BERMEJO (valiente.asun@gmail.com) is an independent consultant and researcher, Barcelona (Spain).

ABSTRACT

This paper presents a mathematical model to forecast the level of residual δ ferrite in terms of FN in austenitic stainless steel welds at cooling rates between 10 ºC/s up to 10^3 ºC/s. With this aim, two series of austenitic steel specimens were prepared using an electric arc remelt furnace. Whilst the alloying level was kept constant at $[Cr_{eq}+Ni_{eq}] = 30$ % and $[Cr_{eq}+Ni_{eq}] = 40$ %, the Cr_{eq}/Ni_{eq} ratio was gradually increased from 1.22 up to 2.00 in each series. For each alloying level, a highly correlated polynomial function (FN vs. Cr_{eq}/Ni_{eq}), was found, being Cr_{eq} and Ni_{eq} Hammar and Svensson's equivalents. These experimental results have led to the importance of $[Cr_{eq}+Ni_{eq}]$ and (Cr_{eq}/Ni_{eq}) variables in the forecast of the residual ferrite content and a general expression including both variables is proposed.

$$FN = 54.22 - 126.26(Cr_{eq} + Ni_{eq}) + [-48.11 + 37.14\,(Cr_{eq} + Ni_{eq})]\left(\frac{Cr_{eq}}{Ni_{eq}}\right) + [-0.23 + 61.95(Cr_{eq} + Ni_{eq})]\left(\frac{Cr_{eq}}{Ni_{eq}}\right)^2$$

The proposed model is able to forecast the level of δ ferrite with a mean error of +1.01 FN within a deviation of +/- 2.12 FN with 95 % probability by just considering the chemical composition of the alloy. This level of error has been proved to be lower than DeLong's and WRC-1988 diagrams errors. Moreover, the proposed model has also been compared with WRC-1992 diagram and FNN-1999 neural network and it provides a more accurate FN forecast within the range of compositions and cooling rates considered.

IIW-Thesaurus keywords: Electric arc, Austenitic Stainless Steels, δ-ferrite, FN, Gas Tungsten Arc Welding (GTAW), Chromium equivalent, Nickel equivalent.

1 Introduction

Controlling the δ-ferrite content in stainless steels is of utmost importance, as its content will influence the material properties and its on-site behaviour in terms of weldability, corrosion resistance, toughness and thermal stability. Hot cracking phenomenon and low temperature toughness have been extensively studied [1-17] and it is commonly agreed that the absence or low δ-ferrite levels, which are the result of austenitic [A] or austenitic-ferritic [AF] solidification modes, leads to hot cracking phenomena during arc welding solidification and also that values over 5 FN are detrimental to low temperature toughness. Therefore, it is vital to control δ-ferrite in those welding consumables which are intended for cryogenic applications. On the other hand, high levels of δ-ferrite coupled with long-time high-temperature cycles may cause embrittlement phenomena due to the spinodal decomposition of δ-ferrite, or the formation of undesirable δ-sigma phase.

The δ-ferrite level can be controlled by taking real measurements, in most cases by using magnetic determination or in the minority by quantitative metallographic determination, or alternatively by using well-recognised forecast methods like the WRC-1992 diagram or the FNN-1999 artificial neural network which are derived from the chemical composition of the weld deposit. These forecast methods are essential during the design stage of a project when the weld pad is not available or when different options of welding consumables are being considered in order to have a good approach of the δ-ferrite level that will be achieved.

Historically, different methods have been used for the forecast of δ-ferrite in stainless steels. In 1985, Olson [18] contributed to the literature with a comprehensive compilation of them. A summarised chronology of the most important events in the δ-ferrite prediction is presented in Table 1.

The current paper presents a new contribution to δ-ferrite prediction in austenitic stainless steel arc-welded metals.

Doc. IIW-2289, recommended for publication by Commission IX "Behaviour of Metals Subjected to Welding."

Table 1 – Summarised chronology of methods for δ-ferrite forecast

Researchers	Year	Event	Significance
Strauss & Maurer [19]	1920	Ni vs. Cr diagram to forecast the metallographic phases in rolled stainless steels.	First diagram to predict metallographic phases in relation to chemical composition in rolled stainless steels.
Newell & Fleischman [20]	1938	First mathematical equation to describe the boundary between austenitic and (γ+δ) mixed microstructure in wrought stainless steels.	Mathematical expressions defining δ-ferrite and γ-austenite phases' stability as a function of the chemical composition of the alloy.
Feild, Bloom & Linnert [21]	1943	Mathematical equation to predict austenitic weld metal microstructure when welding armour steels with austenitic stainless steel consumables.	
Binder, Brown & Franks [22]	1949	Austenite stability versus ferrite stability as a mathematical expression.	
Campbell & Thomas [23]	1946	Microstructure and mechanical properties of welded 25Cr20Ni alloy correlated to chemical composition.	First time proposing the concept of "equivalent", by grouping in the same arm of the expression all the alloying elements promoting the same microstructural phase.
Schaeffler [24-26]	1947-1949	Development of 3 diagrams in which the author gradually refined the Cr equivalent expression. Second and third versions also included iso-ferrite lines expressed as % volume ferrite.	First time of a diagram including Cr equivalent and Ni equivalent on the axes and weld metal microstructural phases plotted, together with ferrite content determined by quantitative metallography.
DeLong & Reid [27, 28]	1956	Diagram focused on the austenite-ferrite transition of Schaeffler's diagram. The influence of the N on the reduction of δ-ferrite content in the weld metal is quantified in the expression of Ni equivalent	Increased the number of austenitic alloys analysed to improve the precision of Schaeffler's diagram. Instead of quantitative metallography, magnetic determination of δ-ferrite was carried out and expressed as % volume ferrite.
Long & DeLong [29-31]	1973	Revision of former diagram including experimental data of alloys with higher δ-ferrite contents than 8 FN to replace previous extrapolations in his former diagram	First time using the new standardised Ferrite Number (FN) scale proposed by the Welding Research Council (WRC) and the International Institute of Welding (IIW)
Between 1973 and 1988 some studies were carried out in relation to the effect of alloying elements on the δ-ferrite content, resulting in new expressions for chromium and nickel equivalents. During that period Suutala *et al.* [2, 3, 6-8] proposed the solidification modes [A, AF, FA, F] and Kotecki [32, 33] found a solution to extend the measurement of δ-ferrite content to the duplex stainless steels			
Siewert, McCowan & Olson [34]	1988	WRC-1988 diagram based on multivariable linear regressions from the WRC database [35] which included the chemical composition and the experimental FN value of 923 stainless steels.	Differently from previous ones, the diagram included duplex and highly alloyed stainless steels data, increasing the forecast to 100 FN and it is the first one in stating the solidification modes and its transition lines instead of the metallographic phases
Kotecki & Siewert [36, 37]	1992	WRC-1992 diagram improved WRC-1988 diagram by adding the Cu contribution to the nickel equivalent in order to extend the diagram to those duplex containing around 2% Cu in their composition.	The diagram was designed with extended axis-similarly to Schaeffler's diagram- in order to make possible the forecast of the chemical composition and the δ-ferrite content of dissimilar welds. This WRC-1992 diagram is still valid in ASME III code
Kotecki [38, 39]	1999	WRC-1992 diagram including the martensite limit formation for 1 %, 4 % and 10 % Mn claddings on it.	Increased the applicability of the WRC-1992 diagram for claddings.
Balmforth & Lippold [40]	2000	Diagram for ferritic and martensitic stainless steels	It depicts microstructures and δ-ferrite (as % ferrite) determined by quantitative metallography (as both martensite and ferrite have magnetic response).
Since the end of the 90's until today, the most significant advance in the prediction of FN has been the development of artificial neural networks. Vasudevan et al. [41] and Vitek et al. [42-45] based their models on multivariable non-linear regressions between the chemical composition, the solidification mode, the cooling rate - which in turn controls the solid state transformation δ→γ- and the FN value. Vitek developed two neural networks, the FNN-1999 considering only the chemical composition as input variable and the ORFN in 2003 including the cooling rate as an additional parameter. Both researchers took the WRC database [35] as input data.			

2 Experimental procedure

Two series of austenitic steel specimens were designed and prepared; the first one consisted of 45 samples with a constant alloying level of $[Cr_{eq}+Ni_{eq}] = 40$ % and the second one consisted of 42 samples with a constant alloying level of $[Cr_{eq}+Ni_{eq}] = 30$ %. Whilst the alloying level was kept constant, the Cr_{eq}/Ni_{eq} ratio was gradually increased from 1.22 up to 2.00 in steps between 0.01 and 0.03. Chromium and Nickel equivalents (Cr_{eq}, Ni_{eq}) were calculated using the equations established by Hammar and Svensson [46] [Equations 1. a), b)]. Suutala ***et al.*** [3, 6-8], who established the solidification modes, also stated that these equivalents gave a better correlation between composition and solidification modes than Schaeffler's or DeLong's ones. Moreover, as it will be shown later in this paper, the use of Hammar and Svensson's equivalents compared with WRC equivalents [36], results in a mathematical model with lower error in the FN prediction.

$$Cr_{eq} = Cr + 1.37\ Mo \quad (1.a)$$

$$Ni_{eq} = Ni + 0.31\ Mn + 22\ C + 14.2\ N \quad (1.b)$$

The base materials used for sample preparation were three grades of solid wires for Gas Tungsten Arc Welding (GTAW), including one mild steel grade and two austenitic grades whose designations and chemical compositions are shown in Table 2. Except for the molybdenum content which was analysed by OES at the author's laboratory, the wires' analyses were conducted by an external and independent laboratory. According to their test report, silicon, manganese, phosphorous, chromium and nickel were analysed by wet process defined in BS Handbook no. 19, BS 6200. Carbon and sulphur were analysed by combustion IR ABS whilst nitrogen and oxygen were analysed by inert gas fusion process.

The pre-cleaned wires were cut into segments between 10-18 mm in length and mixed in required proportions as per Appendixes 1 and 2, so that the designed arc melted samples (buttons) be in accordance with desired levels of $[Cr_{eq}+Ni_{eq}]$ and Cr_{eq}/Ni_{eq} ratios. Later on, in Section 3, these designed compositions will be compared with the experimental compositions determined by Optical Emission Spectroscopy (OES). The total weight of each batch of the samples was 50 g which were melted in a pure argon atmosphere using the electric arc remelt furnace, based on GTAW process which is recommended by the ASTM E1306-94 standard [47] and depicted in Figure 1. In a previous detailed research on the standard by the current author [48], evidences of compositional heterogeneity were found and some modifications were recommended to the ASTM in order to ensure homogeneous samples. Consequently, ASTM issued a new revision to the standard, ASTM E1306-07 [49]. The same work demonstrated that, for a satisfactory sample, the optimum parameters for the remelting process were; -current 550 A, voltage 30 V, holding duration 60 s and then followed by 3 min cooling inside the furnace. Accordingly, these settings were applied to all sample preparation of the current work.

The solid and homogeneous sample obtained was then cut in two halves (see Figure 2) by a cooled and lubricated sawblade and the transversal cross-section (Figure 3), which is considered for δ-ferrite measurements, was slightly ground by using P400 silicon carbide abrasive paper.

As depicted in Figure 3, the transversal cross-section is geometrically characterised by a rectangle of 30 mm length and 7 mm height together with a circular segment of a 30 mm chord and 3 mm height, giving a resulting grid of 12 columns and 5 rows with a minimum of 50 squares each one of an approximate surface of 6 mm^2. The overall surface was divided into three zones containing 12 squares each, as shown in Figure 4: the upper one (coloured in yellow) which was in contact with the inert gas, the lower one (coloured in green) which was in contact with the copper crucible and the central one (coloured in rose) which was considered representative of an as-welded GTAW deposit in terms of cooling rate [48] and therefore was specifically investigated.

An M10B-FE Fischer feritscope was used for the δ-ferrite measurements in terms of Ferrite Number (FN). It was calibrated against a set of IIW (International Institute of Welding) secondary calibration standards according to the international standard EN ISO 8249:2000 [50]. The procedure for the use of the feritscope includes the list of tolerances of the equipment for the different FN bands, and the higher the FN the less stringent the tolerance. Tolerances are as follow: +/- 1FN for (0-14) FN, +/-2 FN for (14-24) FN, +/-3 FN for (24-40) FN and +/-4 FN for (40-70) FN.

Five individual FN measurements were taken at each of the 12 central squares of the transversal cross-section (rose zone in Figure 4); therefore each sample is described by 60 individual readings and its average value.

Table 2 – Chemical composition of the base materials used [wt. %]

AWS designation	Lot	C	Mn	Si	S	P	Cr	Ni	O	N	Mo
ER310	WO11557	0.108	1.70	0.34	0.0018	0.013	25.92	20.65	0.008	0.043	0.06
ER70S-6	WO20929	0.076	1.43	0.81	0.0112	0.011	0.025	0.015	0.010	0.003	0.006
ER312	WO14634	0.105	1.85	0.41	0.0006	0.021	30.31	9.15	0.010	0.151	0.11
ER312	WO11381	0.105	1.80	0.31	0.0005	0.023	30.35	9.12	0.010	0.087	0.20

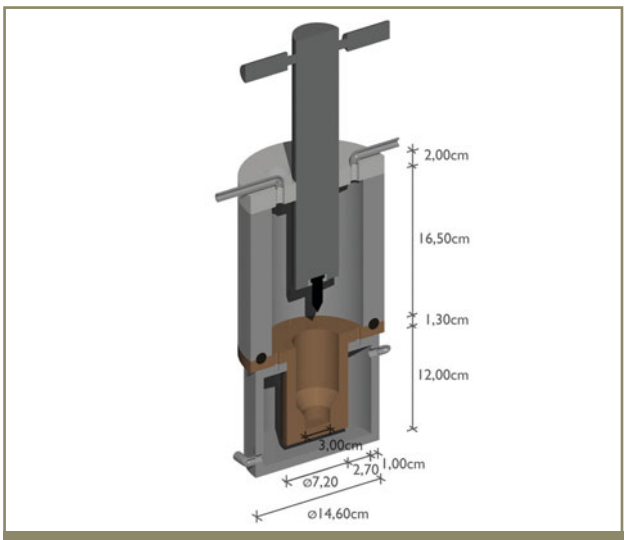

Figure 1 – Schematic illustration of the furnace

To provide with information about variability in these experimental FN measurements, sample A22R (Cr_{eq}/Ni_{eq} = 1.30, [Cr_{eq}+Ni_{eq}] = 40 %) as representative of low ferrite samples and sample A731 (Cr_{eq}/Ni_{eq} = 2.00, [Cr_{eq}+Ni_{eq}] = 40 %) as representative of high ferrite samples were considered. Table 3 shows the results obtained when recording the average FN value and the standard deviation in three specific cells of the central column and also in each zone of the transversal cross-section (Figure 4). In all these cases, the standard deviations of the average values are lower than the feritscope tolerances for the specific FN band, as stated above.

In order to compare the results under a higher cooling rate, the central cross-sections of 6 selected samples for their different solidification modes were additionally remelted, as shown in Figure 5, using a conventional GTAW process with the following parameters: 60 A, 11 V and holding

Figure 2 – Upper and lower half-button surfaces

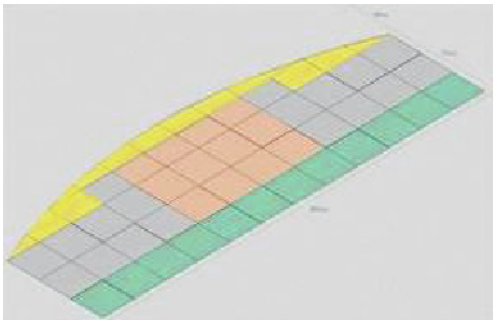

Figure 4 – Transversal cross-section zones: upper (yellow), central (rose) and lower (green)

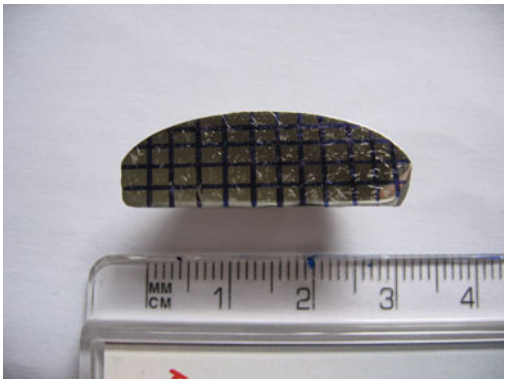

Figure 3 – Transversal cross-section grid for δ-ferrite measurements

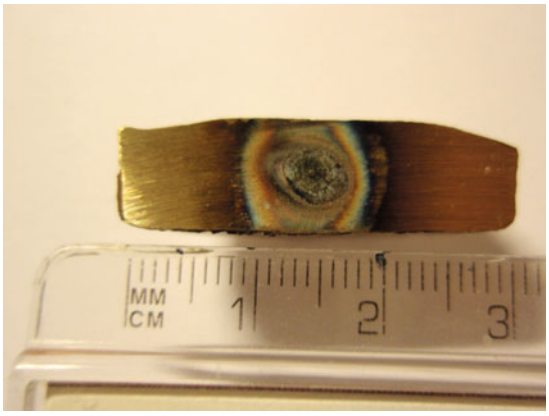

Figure 5 – Macrograph showing the GTAW remelt

Table 3 – Average and standard deviation

Sample	Cell (R1,C6) lower		Cell (R3,C6) central		Cell (R5,C6) upper		Lower transversal cross-section		Central transversal cross-section		Upper transversal cross-section	
	5 readings		5 readings		5 readings		60 readings		60 readings		60 readings	
	$\overline{FN}$	σ	$\overline{FN}$	σ	$\overline{FN}$	σ	$\overline{FN}$	σ	$\overline{FN}$	σ	$\overline{FN}$	σ
A22R	2.32	0.098	1.10	0.109	2.26	0.08	1.35	0.86	1.74	0.44	1.79	0.37
A731	27.56	0.87	38.42	1.92	30.94	1.47	29.79	2.96	36.85	2.99	31.04	2.12

time 15 s, 8 l/min argon gas flow, 14 °C room temperature, 2 % thoriated tungsten diameter 2.4 mm. Twenty FN measurements were taken in the remelted area and the average FN value was calculated.

As has been previously referred, with the aim to check possible variations in the chemical composition caused by vaporization or by segregations during the melting process, samples were analysed by using Optical Emission Spectroscopy with a Spectrolab equipment. One analysis per sample was conducted at the centre of the transversal cross-section.

Table 4 – Average FN at the central zone: series [Cr_{eq} + Ni_{eq}] = 40 %

Sample ref.	Cr_{eq}/Ni_{eq}	FN (60 readings average)
A18	1.22	0.00
A19	1.24	0.06
A20	1.26	0.11
A21	1.28	0.82
A22R	1.30	1.74
A23	1.31	2.27
A24	1.32	3.14
A25	1.34	3.88
A26	1.37	4.39
A27	1.38	5.19
A28R	1.40	5.73
A29	1.42	5.92
A30	1.43	6.80
A31	1.44	7.18
A32	1.46	7.16
A33	1.48	8.04
A34R	1.50	8.36
A35	1.52	8.30
A54R	1.54	11.49
A55R	1.55	12.30
A56R	1.57	11.89
A57R	1.59	14.03
A58R	1.60	13.68
A59R	1.62	13.40
A60	1.64	15.14
A61	1.65	15.24
A62	1.67	16.04
A63	1.68	16.38
A64	1.70	17.57
A65	1.72	18.17
A66R	1.73	19.33
A67R	1.75	21.15
A68R	1.76	23.92
A69R	1.78	22.79
A70R	1.79	23.71
A71R	1.81	23.65
A711	1.83	26.04
A712	1.85	24.77
A713	1.87	25.45
A714	1.89	27.65
A715	1.91	29.27
A716	1.93	30.81
A72R	1.95	34.88
A73	1.97	31.43
A731	2.00	36.85

3 Results and discussion

The individual FN measurements taken on each square of the 87 samples are available in a previous research document by the current author [48]; however Tables 4 and 5 show the average FN value obtained at the central zone of the transversal cross-section for each sample series.

Figure 6 illustrates the relationship between the average FN and the Cr_{eq}/Ni_{eq} ratio shown in Tables 4 and 5. The data are fitted using minimum squares according to a second degree polynomial and the results are depicted graphically on the same Figure 6 and numerically on

Table 5 – Average FN at the central zone: series [Cr_{eq} + Ni_{eq}] = 30 %

Sample ref.	Cr_{eq}/Ni_{eq}	FN (60 readings average)
A36	1.22	0.00
A37	1.24	0.00
A38	1.26	0.00
A39	1.28	0.00
A40R	1.30	0.00
A41	1.31	0.00
A42	1.33	0.00
A43	1.35	0.24
A44	1.37	0.36
A45	1.38	0.48
A46R	1.40	0.96
A47	1.41	0.59
A48	1.43	0.86
A49	1.45	0.89
A50	1.47	1.20
A51	1.48	0.86
A52R	1.50	2.57
A53	1.53	2.07
A531	1.55	4.35
A532	1.57	3.65
A533	1.59	4.41
A74	1.61	3.80
A75	1.63	4.24
A76	1.65	4.87
A77	1.68	6.51
A78	1.70	6.97
A79	1.71	5.44
A80R	1.73	7.20
A81R	1.75	8.40
A82R	1.77	8.81
A83R	1.79	12.33
A84R	1.81	9.01
A85	1.83	9.56
A86	1.85	10.44
A87	1.87	11.98
A88	1.88	10.51
A89	1.90	12.37
A90	1.92	12.90
A91	1.95	13.56
A92	1.96	14.29
A93	1.98	14.34
A94	2.00	16.90

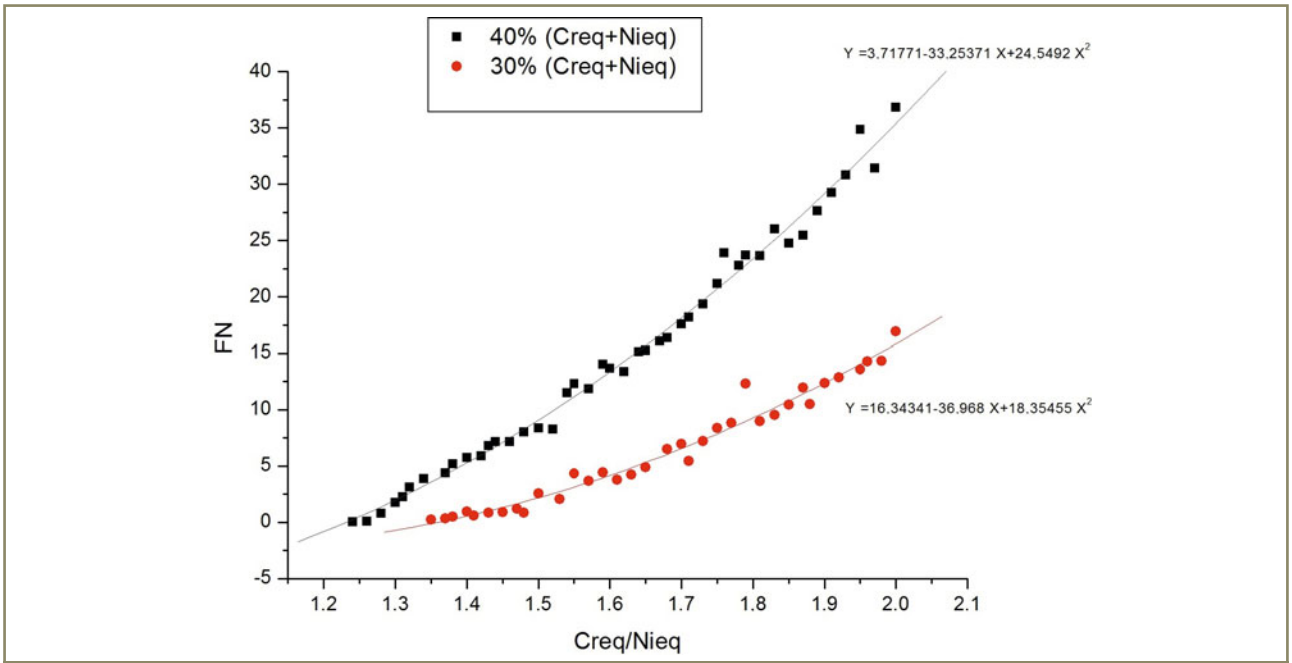

Figure 6 – FN vs. Cr_{eq}/Ni_{eq} and polynomial regression

Table 6. Only those data with FN > 0 have been considered for mathematical fitting. It is clearly shown that the experimental data and the second degree polynomial functions are strongly correlated, as it is demonstrated by the R-square values.

These results demonstrate that for every alloying level $[Cr_{eq}+Ni_{eq}]$ there is a highly correlated polynomial function to fit the experimental FN values and the Cr_{eq}/Ni_{eq} ratio. Therefore, these results lead to the conclusion that FN depends on both variables: the alloying level $[Cr_{eq}+Ni_{eq}]$ and the Cr_{eq}/Ni_{eq} ratio. Taking this point into consideration, a general expression for the FN forecast in the austenitic stainless steels under arc electric solidification conditions is proposed herein.

Variables are defined according to Equation (2) and a general expression is proposed considering the fact that the relationship between variables FN and Cr_{eq}/Ni_{eq} is described by a second degree polynomial function according to Equation (3).

$$\begin{cases} FN = y \\ Cr_{eq}/Ni_{eq} = x \\ Cr_{eq}+Ni_{eq} = z \end{cases} \quad (2)$$

$$\begin{cases} y = a + bx + cx^2 \\ \text{being} \quad a = f(z), b = g(z), c = h(z) \end{cases} \quad (3)$$

Boundary conditions are:

Table 6 – Resulting coefficients for the second degree polynomial regression

Series	a	b	c	R-square
30 %	16.34	-36.97	18.35	0.97
40 %	3.72	-33.25	24.55	0.99

$y = a + b^*x + c^*x^2$, being $y = FN$ and $x = Cr_{eq}/Ni_{eq}$

$y > 0$: the amounts of δ-ferrite are enough to be detected by the feritscope,

$1.22 < x < 2.00$: austenitic stainless steels condition,

$0.2 < z < 0.5$: austenitic stainless steels condition.

The main problem lies in finding the functions f(z), g(z) and h(z) that correlate the variation of the polynomial expression versus the variable z. As the coefficient values are known for z = 0.3 (30 % series) and z = 0.4 (40 % series) (see Table 6), a linear variation of the coefficients is initially assumed (see Equations 4, 5 and 6)

$$f(z) = a = \alpha + \beta z \quad (4)$$

$$g(z) = b = \alpha' + \beta' z \quad (5)$$

$$h(z) = c = \alpha'' + \beta'' z \quad (6)$$

Replacing the pair of known values (a, z) of Table 6 in Equation (4), it leads to a determined 2-equation system which can be solved and as a result, the 2 unknown values (α, β) are calculated. Repeating the same process with the pair of known numbers (b, z) in Equation (5) and (c, z) in Equation (6) it is possible to calculate the remaining unknown values (α′, β′) and (α″, β″).

Equations (7-9) are the result of rewriting Equations (4-6) but introducing the calculated coefficients obtained.

$$f(z) = a = 54.22 - 126.26z \quad (7)$$

$$g(z) = a = -48.11 + 37.14z \quad (8)$$

$$h(z) = a = -0.23 + 61.95z \quad (9)$$

Replacing the above mentioned expressions in the general expression of Equation (3), it is possible to obtain y as

a dependent function of the variables x and z, as it can be seen in Equation (10).

$$y = 54.22 - 126.26\,z + (-48.11 + 37.14z)\,x + (-0.23 + 61.95z)\,x^2 \quad (10)$$

Rewriting Equation (10) but using the physical variables, the general function for predicting the FN in austenitic stainless steels by means of its chemical composition is expressed as Equation (11).

In order to validate the general expression obtained, the WRC database [35] is used. It contains the chemical composition and the FN experimental measurements of 923 different stainless steels, therefore, the Cr_{eq} and Ni_{eq} were calculated from the chemical composition provided by the database and then the $[Cr_{eq}+Ni_{eq}]$ and (Cr_{eq}/Ni_{eq}) values were calculated for each sample and introduced in the Equation (11) in order to obtain a predicted FN value.

Each predicted FN value was then compared with the experimental FN provided by the database and the absolute difference between both values is shown in Figure 7 for the complete set of data.

The statistical processing of the 923 results leads to conclude that the error or absolute difference follows a normal distribution where the expected error is + 2.47 FN with a +/- 5.75 FN confidence interval for 68 % of cases. Considering that the 923 data include all sort of stainless steels (martensitic, ferritic duplex and superaustenitic), and not only the austenitics which are the aim of the current research, it can be concluded that the dispersion between the predicted FN by the Equation (11) and the experimental FN stated by the WRC is acceptable.

However, as depicted in Figure 8, if the comparison is done but only considering the 279 samples of the database whose chemical compositions are within the range of the

$$FN = 54.22 - 126.26(Cr_{eq} + Ni_{eq}) + [-48.11 + 37.14\,(Cr_{eq} + Ni_{eq})]\left(\frac{Cr_{eq}}{Ni_{eq}}\right) + [-0.23 + 61.95(Cr_{eq} + Ni_{eq})]\left(\frac{Cr_{eq}}{Ni_{eq}}\right)^2 \quad (11)$$

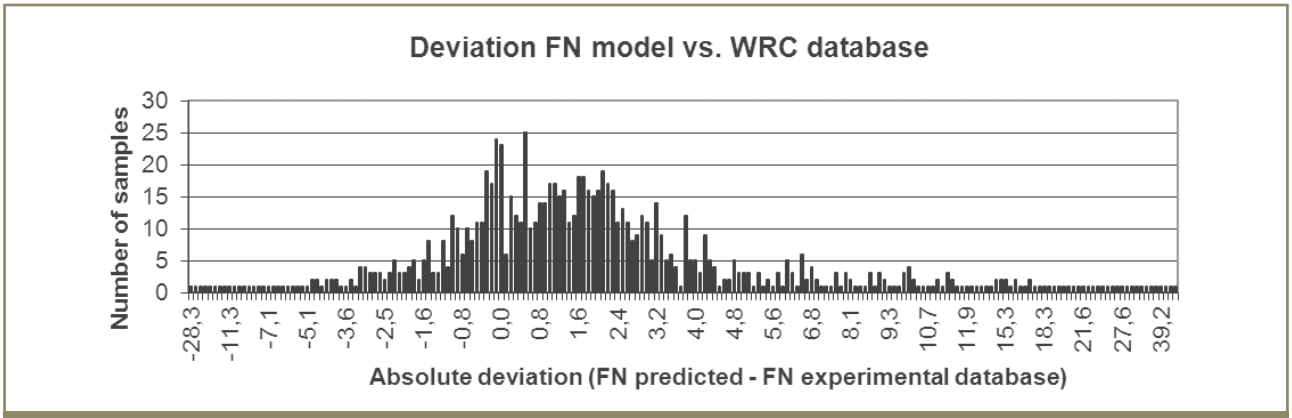

Figure 7 – Frequency histogram showing the absolute difference between the predicted FN and the experimental FN (923 data)

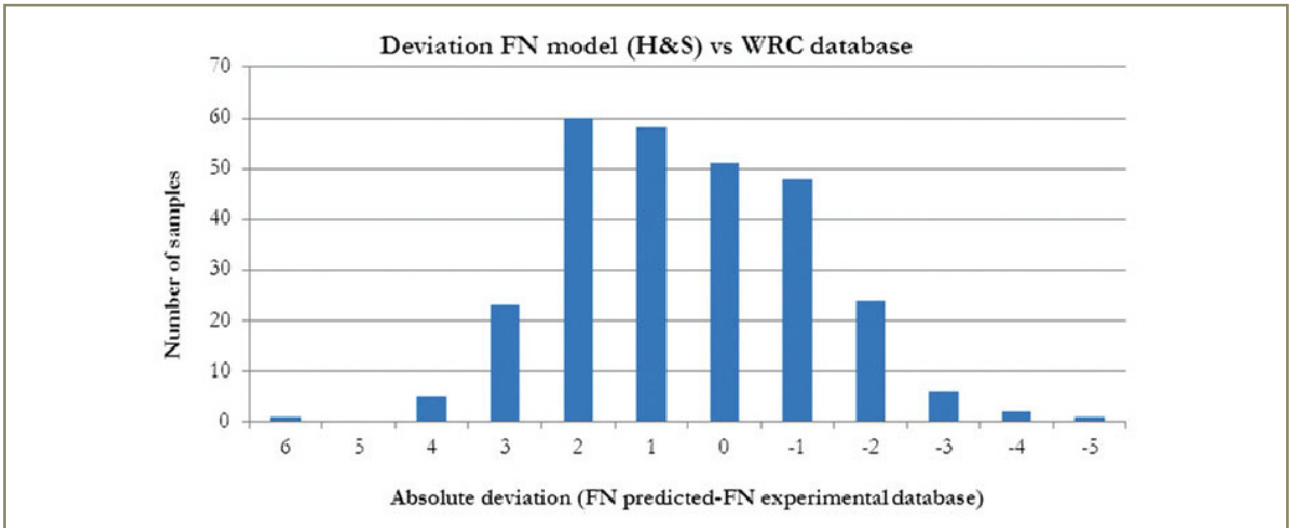

Figure 8 – Frequency histogram showing the absolute difference between the predicted FN and the experimental FN (279 austenitic samples)

austenitics [Cr: 19-27 %, Ni: 6.6-20 %, Mn: 1-2 %, C: 0.02-0.08 %, Mo: 0-2 %, N < 0.15 %], then the statistical processing confirms that the expected error is **+ 1.01 FN** with a +/- 1.06 FN interval confidence for 68 % of cases and a **+/- 2.12 FN interval confidence for a probability of 95 %**. Therefore, the general expression provides for 95 % of samples an error better than 1.01 FN +/- 2.12 FN.

This level of error given by the general expression has been compared with DeLong Diagram's error and with WRC-1988 Diagram's error [34, 35, 51]. As it is shown in Figure 9, for the FN range between (0-18), DeLong's histogram is claimed to be centred in an error of +2 FN with a +/-8 FN interval confidence, and for the same FN range, the WRC-1988 is claimed to be centred in -1 FN with a +/-4 FN for an interval confidence of 95 %. These are higher errors than the obtained with the general expression proposed here.

The author recognises that the proposed mathematical model is based on the measurements taken by one single feritscope and on the chemical analysis of one single laboratory, and that although these equipments are properly calibrated, they could be subjected to a degree of uncertainty compared to the results given by a different equipment or laboratory. However, the fact that the mathematical model has been successfully contrasted with the experimental values given by the WRC database, which contains data from very different sources, it contributes to validate the mathematical model proposed herein.

It is well known that nowadays the most accurate methods for the FN forecast in arc welding are the WRC-1992 Diagram and the FNN-1999 neural network, therefore, in order to compare the accuracy and goodness between the above mentioned methods and the general expression found in this research, the chemical composition of 87 samples

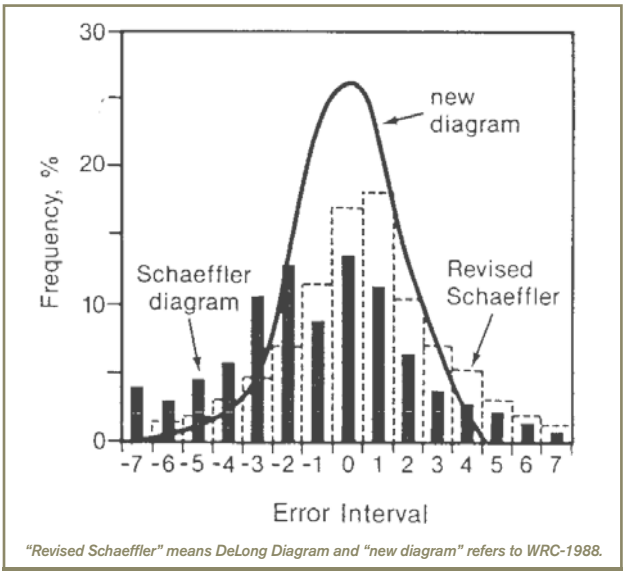

"Revised Schaeffler" means DeLong Diagram and "new diagram" refers to WRC-1988.

Figure 9 – Histograms of WRC-1988/DeLong/Schaeffler's diagrams [35]

prepared in this research were used as input data for the three methods and results are depicted in Figure 10. The dotted red line represents the ideal method, where the experimental and the calculated FN values match. The rose circles represent the correlation between the experimental FN and the predicted FN by the WRC-1992 diagram, whilst the orange triangles refer to the FNN-1999 neural network and the green squares represent the correlation of the general expression proposed here. It is shown that the WRC-1992 underestimates the FN value throughout all the compositions range whilst the FNN-1999 makes an accurate forecast for samples with FN < 10 and that similarly to WRC-1992, the method also underestimates the values for samples with FN >15. It is clear that the general expression (Equation 11) provides better matching than WRC-1992 and FNN-1999 for these 87 samples.

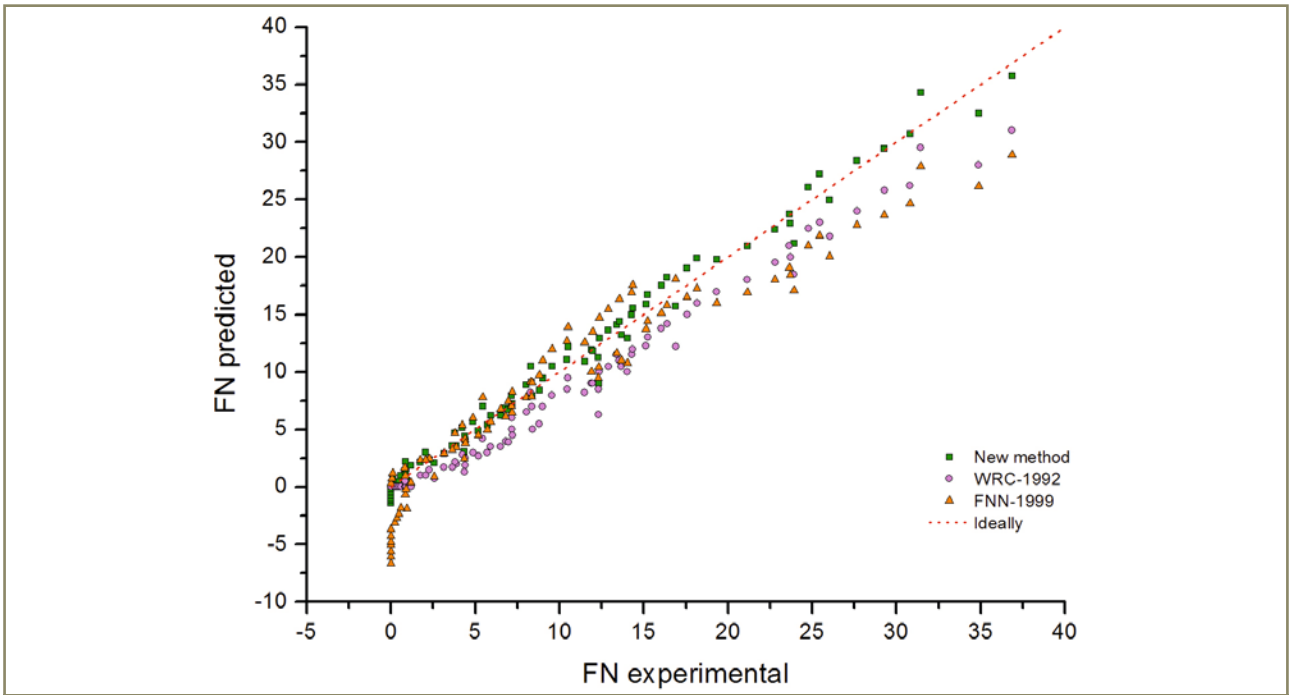

Figure 10 – Comparison between forecast methods: General expression, WRC-1992 Diagram and FNN-1999 neural network

In a previous research work by the current author [48], it was determined by DAS (Dendrite Arm Spacing) that these samples prepared using the electric arc furnace were cooled at 10ºC/s whilst the central area remelted using conventional GTAW was cooled at 10^2-10^3 ºC/s. Cooling rates in the orders of magnitude between 10-10^3 ºC/s are considered typical for the arc welding processes [52-54]. Table 7 shows the experimental FN measurements taken in both cooling conditions and also the FN values obtained using the general expression [Equation (11)]. It is clearly shown that the general expression provides an excellent forecast for the FN value under both cooling conditions. The only case where the forecast differs from the experimental measurements is in the specific case of the sample with primary ferritic solidification mode [F], which is more related to the duplex stainless steels than to the austenitics. The cooling rate highly influences the presence of residual δ-ferrite at room temperature in primary ferritic modes [F] because high cooling rates limit the diffusion and the solid state transformation δ → γ, therefore it is logical to observe higher FN values at higher cooling rates as long as the working conditions will be in the order of magnitude of the arc electric cooling rates. However, under extremely high cooling conditions (10^4-10^7 ºC/s) usually related to Laser Beam Welding or Electron Beam Welding, researchers found that those samples which would present [F] solidification mode under arc welding cooling rates, turn to present γ-austenite as stable phase at room temperature. Elmer et *al.* [53, 55], Anderson ***et al.*** [56] and Inoue *et al.* [57] propose that samples with ferritic primary solidification mode [F] under high cooling conditions could experience δ → γ massive transformation, whilst other researchers [58] also explain the lack of δ-ferrite at room temperature by a shift from [F] to [A] solidification mode caused by the dendrite tip undercooling phenomenon.

A thorough mathematical development of Equation (11) has been carried out in previous research work [48], and other practical and additional results related to the design of austenitic alloys have been proposed, for example it is possible to know for whatever alloying level [Cr_{eq}+Ni_{eq}] which would be the minimum Cr_{eq}/Ni_{eq} ratio to detect δ-ferrite (see Equation (12)), or inversely for a fixed Cr_{eq}/Ni_{eq} ratio, it would be possible to find the linear expression which defines the FN value versus the alloying level.

In order to check any possible influence of the arc melting process on the chemical composition of the samples, a comparison has been established between the designed compositions, which were calculated from the experimental composition of the initial wires (see Table 2 and Appendices 3 and 4), and the buttons' compositions which were determined by Optical Emission Spectroscopy (see Appendices 5 and 6). One analysis per sample was conducted at the centre of the transversal cross-section.

With this aim, a deviation ratio (ε) was defined as the quotient between the experimental composition and the designed composition. Therefore, elements with ε =1 indicate that there is no deviation between their initially designed composition and the experimental one in the area analysed, whilst ε >1 and ε <1 indicate a local increase or loss respectively. Figure 11 summarises the results obtained.

The experimental values for nitrogen and oxygen obtained by OES are abnormally high (Appendixes 5 and 6), giving ε values up to 8, so they cannot be considered for any further discussion and this also prevents the calculation of experimental Ni_{eq} values and their possible comparison with the initially designed Ni_{eq} values. When plotting the nitrogen and oxygen deviations, it was found that both elements present the same trend in the same samples, and from metallographic inspection nor oxides nor nitrides are observed in the samples, therefore, these facts seem to indicate that the difference in dimensions between the sample and the spectrometer fixture has allowed some air to enter into the analysis chamber, giving these abnormally high values for nitrogen and oxygen.

$$Cr_{eq}/Ni_{eq} = \frac{48.11-37.14\,(Cr_{eq}+Ni_{eq})+\sqrt{2364.45-17125.49\,(Cr_{eq}+Ni_{eq})+32666.61(Cr_{eq}+Ni_{eq})^2}}{123.90\,(Cr_{eq}+Ni_{eq})-0.46} \quad (12)$$

Table 7 – Predicted FN values vs. measured FN at different cooling rates

Sample ref.	Cr_{eq}/Ni_{eq}	[Cr_{eq}+Ni_{eq}]	Solidif. Mode [48]	Avg FN GTAW Experim. V_R= 10^2-10^3 °C/s	FN forecast (Equation 11)	Avg. FN furnace Experim. V_R= 10 °C/s	Feritscope error
A39	1.28	30 %	A	0.0	(-0.9)	0.0	+/- 1
A42	1.33	30 %	AF	0.01	(-0.4)	0.0	+/- 1
A21	1.28	40 %	AF/FA	0.6	1.4	0.8	+/- 1
A74	1.61	30 %	FA	3.7	4.4	3.8	+/- 1
A57R	1.59	40 %	FA	12.8	12.9	14.0	+/- 1
A94	2.00	30 %	FA/F	20.4	15.8	16.9	+/- 2
A731	2.00	40 %	F	60.5	35.4	36.8	+/- 5

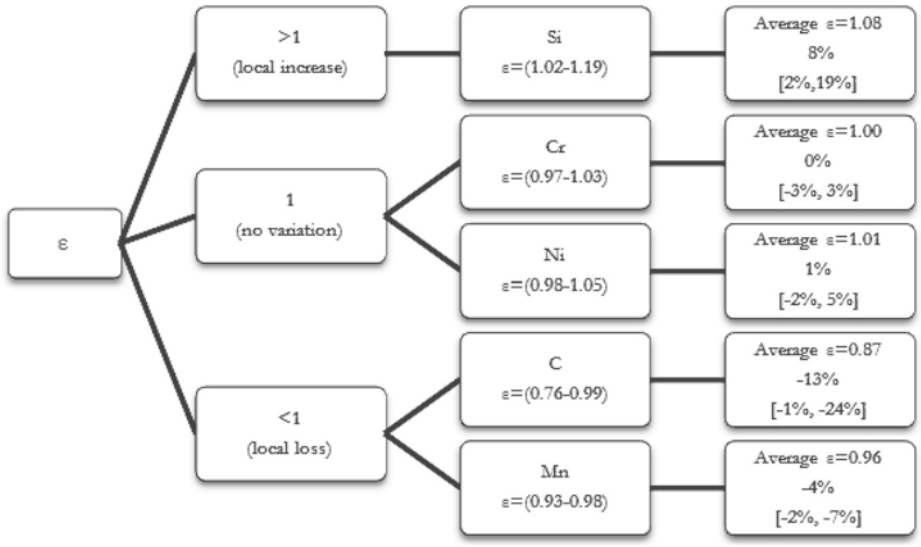

Figure 11 – Deviation ratios for the chemical composition of the samples

Regarding silicon, it does not have a specific weight in the Hammar & Svensson's equivalents, but a local increase was evident. By using SEM microscopy and EDS microanalysis, the current author [48] found clear evidences of spherical particles of one micrometre diameter which were mainly enriched in silicon and in minor contribution included sulphur and traces of aluminium. From 2 to 3 particles were found in an area of 40 x 60 μm. Therefore, it seems very possible that OES analysis shows a local increase in silicon due to this segregation phenomenon.

Carbon and manganese experience a loss during the melting process which has been previously related to vaporization by some authors [59-62], however, considering the relative weight that carbon and manganese have in the calculation of the Hammar & Svensson's nickel equivalent and considering also the low initial contents of these elements, it is possible to demonstrate that a reduction of 13 % in carbon and of a 4 % in manganese do not influence on the initially designed value of nickel equivalent.

Chromium and nickel, which are the main responsible elements for the δ-ferrite content and which have the most important contribution to the calculation of the equivalents, do not experience a significant variation in their chemical composition (average $\varepsilon_{Cr} = 1.00$ and $\varepsilon_{Ni} = 1.01$) due to the arc melting process. From the above mentioned results, it is possible to conclude that the initially designed Cr_{eq}/Ni_{eq} ratios remain unchanged despite the melting process.

The currently developed mathematical model uses the Hammar & Svensson's equivalents. Below, the same mathematical procedure was applied again, but this time using three different equivalents as input data and

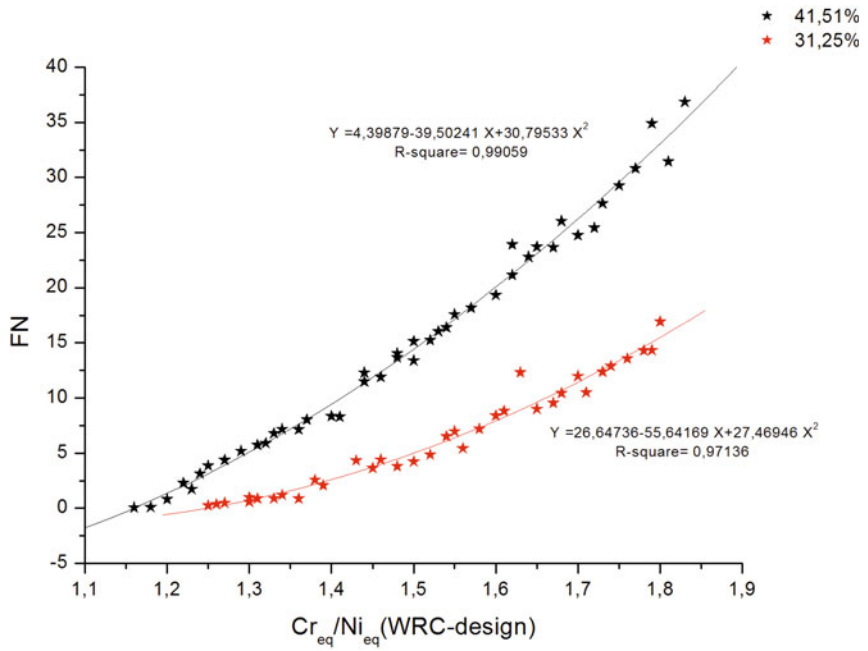

Figure 12 – FN vs. Cr_{eq}/Ni_{eq} (WRC)

consequently obtaining three new mathematical expressions. Therefore, firstly experimental FN vs. each different $Cr_{eq}X/Ni_{eq}X$ were plotted and second degree polynomial fit were interpolated, secondly the general second degree polynomial function was calculated and finally, the general function obtained was validated by comparison between the predicted FN and the WRC experimental database. The equivalents used as input data were: the current WRC equivalents [36], the chromium and nickel values obtained from OES analysis of the samples and finally, the chromium and nickel values designed from weight combination of the initial wires. Figures 12, 13 and 14 illustrate the relationship between the experimental FN values and the above mentioned equivalent ratios. As

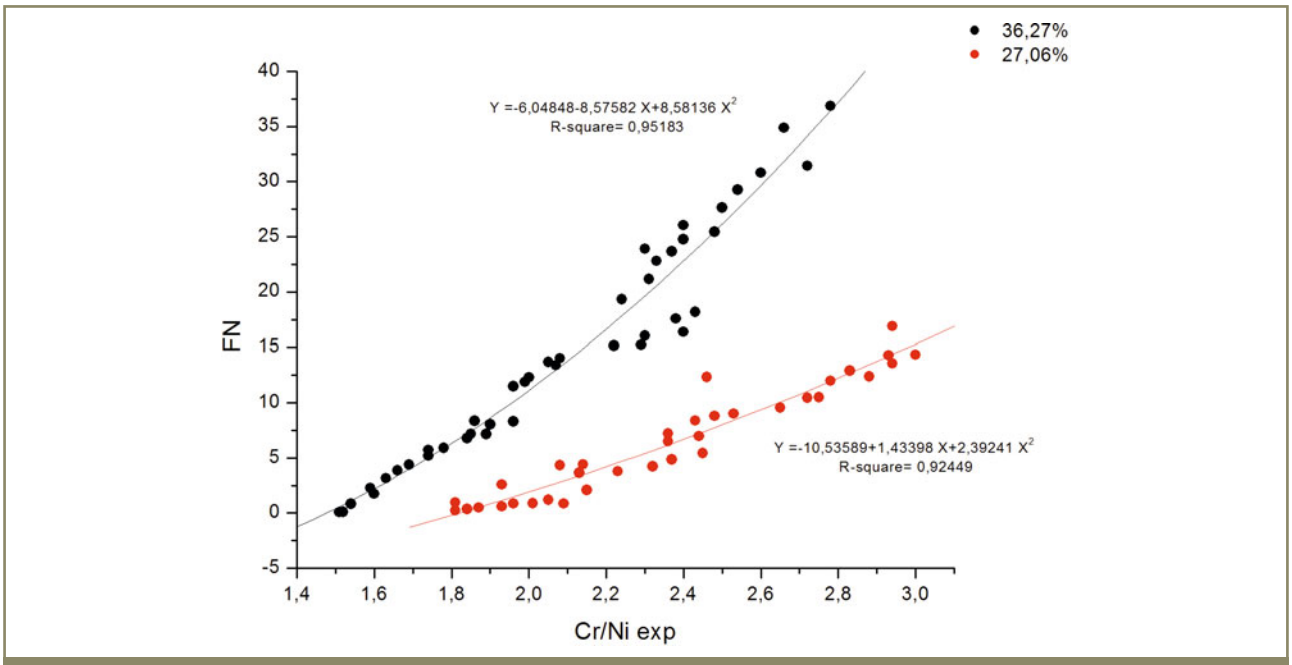

Figure 13 – FN vs. Cr/Ni (OES)

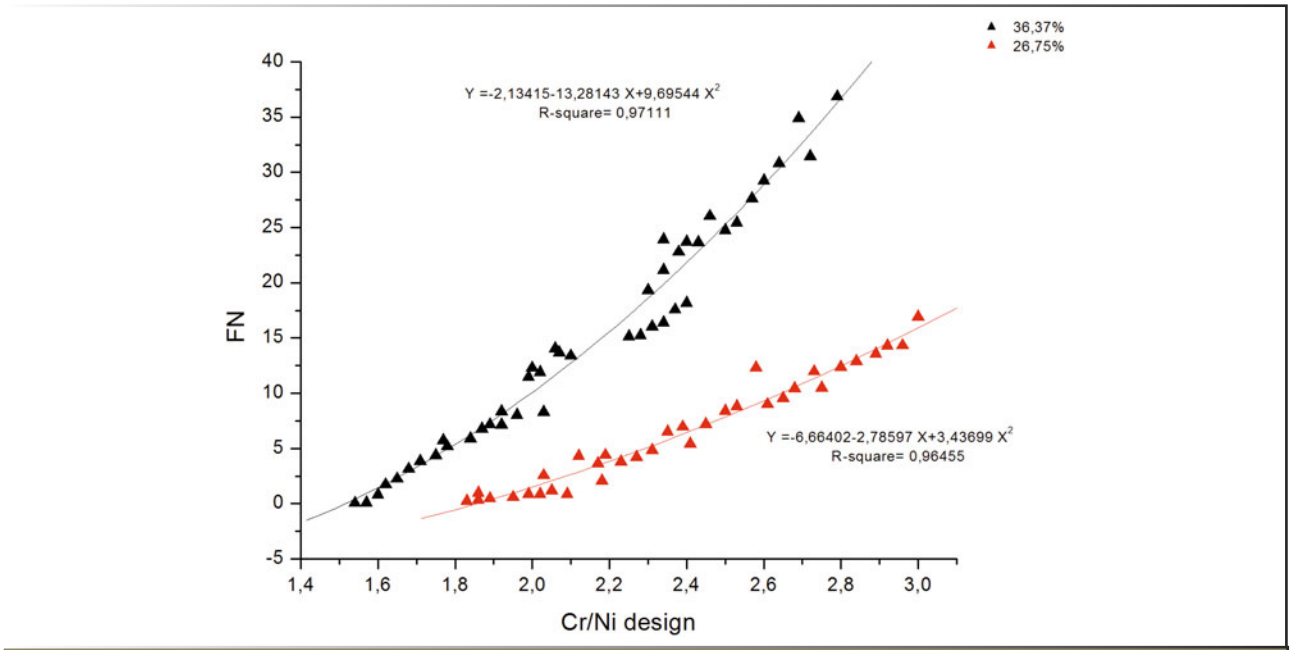

Figure 14 – FN vs. Cr/Ni (Designed)

Table 8 – Error comparison with different models

Equivalents	Expected error (Average error)	Confidence interval for a probability of 68 %	Confidence interval for a probability of 95 %
WRC	**2.45 FN**	**+/- 1.00 FN**	**+/- 2.00 FN**
OES Cr, Ni	-1.29 FN	+/- 2.38 FN	+/- 4.76 FN
Designed Cr, Ni	-1.96 FN	+/- 3.07 FN	+/- 6.14 FN

depicted, data were fitted using minimum squares to second degree polynomial functions and similarly to Figure 6 with Hammar and Svensson's equivalents, a strong correlation (R-square) was found in all the cases, independently of the equivalents used.

It is worthy to note that the best correlations are found when using Hammar and Svensson's and WRC equivalents, even with the same R-square values. Therefore, as it was foreseeable, the use of equivalents rather than only Cr and Ni compositions confirms the influence of the alloying elements –ferrite promoters and austenite promoters- on the FN values.

The general second degree polynomial functions found for each of the three above mentioned cases are Equation (13) for WRC equivalents, Equation (14) for OES (Cr, Ni) compositions and Equation (15) for designed (Cr, Ni) compositions.

In order to validate these expressions, the predicted FN values were compared against the 279 austenitic samples of the WRC experimental database [35]. Results are summarised in Table 8 and from the three different equivalents evaluated, it seems clear that the model with the WRC ones presents the best ones with the lowest confidence interval. However, as it was noted previously, the currently developed model with Hammar and Svensson's equivalents has an expected error of **+1.01 FN, a +/-1.06 FN interval confidence for 68 % cases and a +/- 2.12 FN interval confidence for 95 % cases**. When comparing it with the model obtained with WRC equivalents, it is clear that there is no significant difference in terms of confidence intervals, but there is a higher expected error (+2.45 FN) in the model with WRC equivalents. Therefore, it could be concluded that the mathematical expression with Hammar and Svensson's equivalents results in the lower error for FN prediction.

$$FN = 94.41 - 216.85(Cr_{eq} + Ni_{eq}) + [-104.80 + 157.30\,(Cr_{eq} + Ni_{eq})]\left(\frac{Cr_{eq}}{Ni_{eq}}\right) + [17.34 + 32.42(Cr_{eq} + Ni_{eq})]\left(\frac{Cr_{eq}}{Ni_{eq}}\right)^2 \quad (13)$$

$$FN = -23.72 + 48.72(Cr + Ni) + [30.84 - 108.68\,(Cr + Ni)]\left(\frac{Cr}{Ni}\right) + [-15.79 + 67.20(Cr + Ni)]\left(\frac{Cr}{Ni}\right)^2 \quad (14)$$

$$FN = -19.26 + 47.09(Cr + Ni) + [26.40 - 109.10\,(Cr + Ni)]\left(\frac{Cr}{Ni}\right) + [-13.97 + 65.06(Cr + Ni)]\left(\frac{Cr}{Ni}\right)^2 \quad (15)$$

4 Conclusion

It has been found that the δ-ferrite content (expressed as FN) versus the Cr_{eq}/Ni_{eq} ratio can be mathematically fitted by a highly correlated second degree polynomial for each constant alloying level $[Cr_{eq}+Ni_{eq}]$:

$FN = 16.34 - 36.97(Cr_{eq}/Ni_{eq}) + 18.35(Cr_{eq}/Ni_{eq})^2$
for $[Cr_{eq}+Ni_{eq}] = 30$ %

$FN = 3.72 - 33.25(Cr_{eq}/Ni_{eq}) + 24.55(Cr_{eq}/Ni_{eq})^2$
for $[Cr_{eq}+Ni_{eq}] = 40$ %

Based on these results, a general expression has been developed in order to propose a new tool to forecast the level of δ-ferrite in the austenitic stainless steels (from FN = 0 up to FN = 37) under arc electric solidification conditions (cooling rates from 10°C/s up to 10^3 °C/s), just by using the chemical composition as input data.

$$FN = 54.22 - 126.26(Cr_{eq} + Ni_{eq}) + [-48.11 + 37.14\,(Cr_{eq} + Ni_{eq})]\left(\frac{Cr_{eq}}{Ni_{eq}}\right) + [-0.23 + 61.95(Cr_{eq} + Ni_{eq})]\left(\frac{Cr_{eq}}{Ni_{eq}}\right)^2$$

Being Cr_{eq} and Ni_{eq} Hammar & Svensson's equivalents.

It has been demonstrated that the expression gives a forecasted FN value which could differ from the experimental value between -1.11 and +3.13 with 95 % confidence interval. This is an excellent level of error taking into consideration that other highly recognised methods like DeLong Diagram claimed to present an error of +/-8 FN or WRC-1988 Diagram which claimed to present a deviation of +/-4 FN for the same confidence level. On the other hand, the FN values predicted by the expression found in this research present less deviation than the predictions made for the same samples using the currently international methods WRC-1992 Diagram and FNN-1999 neural network, and moreover its use only needs the input of the Cr_{eq} and the Ni_{eq} in the general expression, which is simpler than using a diagram or running a neural network in a computer.

It has been found that the model with Hammar and Svensson's equivalents results in the lower error for FN predictions in comparison with WRC equivalents and in comparison with equivalents considering only Cr and Ni compositions (even if they are designed compositions or determined by OES). It is also worthy to notice that FN versus Cr_{eq}/Ni_{eq} follows second degree polynomial functions for a constant level of alloy $[Cr_{eq}+Ni_{eq}]$ independently from the equivalents used.

The mathematical processing of the general expression has led to find other mathematical expressions of interest in the austenitic stainless steel design, for example in the

cryogenic field where δ-ferrite needs to be carefully controlled. Therefore, it is possible to calculate the chemical composition boundaries for base materials and welding consumables in order to achieve low levels of δ-ferrite.

The general expression proposed in this work also provides an excellent forecast for FN in austenitic stainless steels in the range of cooling rates of 10^2-10^3 °C/s. The only case where the forecast differs from the experimental measurements is in the specific case of the sample with primary ferritic solidification mode [F], which is more related to the duplex stainless steels than to the austenitics.

Acknowledgements

The author gratefully acknowledges the support of Metrode Products Ltd and is especially indebted to Dr. Zhuyao Zhang and Mr. Adam W. Marshall for providing the materials and facilities in order to carry out this research. The current research is part of the Doctoral Degree Thesis entitled "Modelització del nivell de ferrita δ als acers inoxidables austenítics sotmesos a fusió per arc electric", which was submitted for the Degree of Doctor in Chemistry by the author at the University of Barcelona the 29th of June 2010. It is also gratefully acknowledged the supervision of Dr. Pere Molera and Dr. Núria Llorca from the Department of Materials Science and Metallurgical Engineering at the University of Barcelona. It is gratefully acknowledged the sponsorship by ESAB for the author's attendance to the IIW 64th Annual Assembly in Chennai and is especially grateful to Dr. Leif Karlsson for his invaluable commitment.

References

[1] Kujanpää V.P. and David S.A.: White, C.L. Formation of hot cracks in austenitic stainless steel welds- solidification cracking, Welding Journal, 1986, vol. 65, no. 8, pp. 203s-212s.

[2] Suutala N., Takalo T. and Moisio T. The relationship between solidification and microstructure in austenitic and austenitic-ferritic stainless steel welds, Metallurgical Transactions A. 1979, vol. 10A, no. 4, pp. 512-514.

[3] Kujanpää V.P., Suutala N, Takalo T. and Moisio T. : Correlation between solidification cracking and microstructure in austenitic and austenitic-ferritic stainless steel welds, Welding Research International, 1979, vol. 9, no. 2, pp. 55-75.

[4] Lippold J.C. and Savage W.F.: Solidification of austenitic stainless steel weldments: Part III – The effect of solidification behavior on hot cracking susceptibility, Welding Journal, 1982, no. 12, pp. 388s-396s.

[5] Brooks J.A., Thomson A.W. and Williams J.C.: Variations in weld ferrite content due to P and S, Welding Journal, 1983, no. 8, pp. 220s-225s.

[6] Kujanpää V.P, Suutala N.J., Takalo T.K. and Moisio T.J.I.: Solidification cracking – estimation of the susceptibility of austenitic and austenitic-ferritic stainless steel welds, Metal Construction, 1980, vol. 12, no. 6, pp. 282-285.

[7] Suutala N, Takalo T. and Moisio T.: Technical note: Comment on the transformation $\delta \rightarrow \gamma$ by a massive mechanism in austenitic stainless steel, Welding Journal, 1981, no. 5, pp. 92s-93s.

[8] Suutala N.: Effect of solidification conditions on the solidification mode in austenitic stainless steels, Metallurgical Transactions A., 1983, vol. 14A, no. 2, pp. 191-197.

[9] Kujanpää V.P.: Effects of steel type and impurities in solidification cracking of austenitic stainless steel welds, Metal Construction, 1985, vol. 17, no. 1, pp. 40R-46R.

[10] Brooks J.A.: Solidification behavior and cracking susceptibility of austenitic stainless steel welds, Proceedings of the 8th Annual North American Welding Research Conference, Columbus, Ohio, October 1992, pp. 19-21.

[11] Li L. and Messler R.W. Jr.: The effects of phosphorus and sulphur on susceptibility to weld hot cracking in austenitic stainless steels, Welding Journal, 1999, no. 12, pp. 387s-396s.

[12] Brooks J.A, Robino C.V., Headley T.J and Michael J.R.: Weld solidification and cracking behavior of free-machining stainless steel, Welding Journal, 2003, no. 3, pp. 51s-64s.

[13] Brooks J.A., Goods S.H. and Robino C.V. Weld properties of AISI 303 free-machining stainless steel, Welding Journal, 2003, no. 4, pp. 84s-92s.

[14] Shankar V., Gill T.P.S, Mannan S.L and Sundaresan S.: Solidification cracking in austenitic stainless steel welds, Sadhana, 2003, vol. 28, pp. 359-382.

[15] Katayama S., Fujimoto T. and Matsunawa A.: Correlation among solidification process, microstructure, microsegregation and solidification cracking susceptibility in stainless steel weld metals, Transactions of Japanese Welding Research Institute, 1985, vol. 14, no. 1, pp. 123-138.

[16] Lundin C.D., Delong W.T. and Spond D.F.: Ferrite-fissuring relationship in austenitic stainless steel weld metals, Welding Journal, 1975, no. 8, pp. 241s-246s.

[17] Lundin C.D., Delong W.T. and Spond D.F.: The fissure bend test, Welding Journal, 1976, no. 6, pp. 145s-151s.

[18] Olson D.L.: Prediction of austenitic weld metal microstructure and properties, Welding Journal, 1985, vol. 64, no. 10, pp. 281s-295s.

[19] Strauss B. and Maurer E.: Die Hochlegierten Chromnickelstahle als nichtrostende Stahle. Kruppsche Monatshefte, 1920, vol. 1, no. 8, pp. 129-146.

[20] Newell H.D. and Fleischmann M.: Hot rolled metal article and method of making same, U.S. patent n° 2-118-683, 1938.

[21] Feild A.L., Bloom K.F. and Linnert G.E.: Development of armor welding electrodes: relation of the composition of austenitic (20Cr-10Ni) electrodes to the physical and ballistic properties of armor weldments, OSRD Report n° 1636, 1943.

[22] Binder W.O., Brown C.M. and Franks R.: Resistance to sensitization of austenitic chromium-nickel steels of 0.03% max. carbon content, Trans. ASM., 1949, vol. 41, pp. 1301-1346.

[23] Campbell H.C. and Thomas Jr. R.D.: The effect of alloying elements on the tensile properties of 25-20 weld metal, Welding Journal, 1946, vol. 25, no. 11, pp. 760s-768s.

[24] Schaeffler A.L.: Selection of austenitic electrodes for welding dissimilar metals, Welding Journal, 1947, vol. 26, no. 10, pp. 1-20.

[25] Schaeffler A.L.: Welding dissimilar metals with stainless electrodes, Iron Age, 1948, vol. 162, pp. 72.

[26] Schaeffler A.L.: Constitution diagram for stainless steel weld metal, Metal Progress, 1949, vol. 56, no. 11, pp. 680-680B.

[27] Delong W.T. and Reid Jr. H.F.: Properties of austenitic chromium in austenitic chromium-manganese stainless steel weld metal, Welding Journal, 1957, vol. 37, no. 1, pp. 1-8.

[28] Delong W.T.: A modified phase diagram for stainless steel weld metals, Metal Progress, 1960, vol. 77, no. 2, pp. 99-100B.

[29] Long C.J. and Delong W.T.: The ferrite content of austenitic stainless steel weld metal, Welding Journal, 1973, vol. 52, no. 7, pp. 281s-297s.

[30] Delong W.T.: Ferrite in austenitic stainless steel weld metal, Welding Journal, 1974, no. 7, pp. 273s-286s.

[31] Reid H.F. and Delong W.T.: Making sense out of ferrite requirements in welding stainless steels, Metal Progress, 1973, no. 6, pp. 73-77.

[32] Kotecki D.J.: Extension of the WRC Ferrite Number system, Welding Journal, 1982, vol. 61, no. 11, pp. 352s-361s.

[33] Kotecki D.J.: Ferrite control in duplex stainless steel weld metal, Welding Journal, 1986, no. 10, pp. 273s-278s.

[34] Siewer T.A., McCowan C.N. and Olson D.L.: Ferrite Number prediction to 100 FN in stainless steel weld metal, Welding Journal, 1988, vol. 67, no. 12, pp. 289s-298s.

[35] McCowan C.N., Siewert T.A and Olson D.L.: Stainless steel weld metal: Prediction of ferrite content, WRC Bulletin, 1989, no. 342, 36 pages.

[36] Kotecki D.J. and Siewert T.A.: WRC-1992 Constitution Diagram for stainless steel weld metals: a modification of the WRC-1988 Diagram, Welding Journal, 1992, no. 5, pp. 171s-178s.

[37] Feldstein J.: The WRC Diagram, Svetsaren,1993, vol. 47, no. 2, pp. 36-39.

[38] Kotecki D.J.: A martensite boundary on the WRC-1992 diagram, Welding Journal, 1999, vol. 78, no. 5, pp. 181s-192s.

[39] Kotecki D.J.: Martensite prediction in stainless steel weld cladding, Paper presented at the Stainless Steel World Conference, 1999, no. 2, pp. 573-583.

[40] Balmforth M.C. and Lippold J.C.: A new ferritic-martensitic stainless steel constitution diagram, Welding Journal, 2000, vol. 79, no. 12, pp. 339s-345s.

[41] Vasudevan M., Murugananth M. and Bhaduri A.K.: Application of Bayesian neural network for modeling and prediction of ferrite number in austenitic stainless steel welds, On line, Retrieved November 2nd 2004, Available at: http://www.msm.cam.ac.uk/phase-trans/2001/Ferrite_number.pdf.

[42] Vitek J.M., Iskander Y.S., Oblow E.M. : Improved ferrite number prediction in stainless steel arc welds using artificial neural networks – part 1: neural network development, Welding Journal, 2000, no. 2, pp. 33s-40s.

[43] Vitek J.M., Iskander Y.S. and Oblow E.M.: Improved ferrite number prediction in stainless steel arc welds using artificial neural networks – part 2: neural network results, Welding Journal, 2000, no. 2, pp. 41s-50s.

[44] Vitek J.M., David S.A. and Hinman C.R.: Improved ferrite number prediction model that accounts for cooling rate effects – part 1: model development, Welding Journal, 2003, no. 1, pp. 10s-17s.

[45] Vitek J.M., David S.A., Hinman C.R.: Improved ferrite number prediction model that accounts for cooling rate effects- Part 2: model results, Welding Journal, 2003, no. 2, pp. 43s-50s.

[46] Hammar Ö. and Svensson U.: Influence of steel composition on segregation and microstructure during solidification of austenitic stainless steels, Solidification and casting of metals, Conference, The Metals Society, 1979, pp. 401-410.

[47] ASTM E1306-94 (Reapproved 2004) Standard Practice for Preparation of Metal and Alloy Samples by Electric Arc Remelting for the Determination of Chemical Composition, Philadelphia: ASTM International, 2004.

[48] Valiente Bermejo M.A.: Modelització del nivell de ferrita δ (FN) als acers inoxidables austenítics sotmesos a fusió per arc electric, Modelization of δ-ferrite content (FN) in austenitic stainless steels under electric arc conditions, PhD. University of Barcelona, Department of Materials Science and Metallurgical Engineering, June 2010, ISBN 978-84-693-5713-2 (in Catalan).

[49] ASTM E1306-07 Standard practice for preparation of metal and alloy samples by electric arc remelting for the determination of chemical composition, Philadelphia: ASTM International, 2007.

[50] EN ISO 8249:2000, Welding, Determination of Ferrite Number (FN) in austenitic and duplex ferritic-austenitic Cr-Ni stainless steel weld metals, 2000.

[51] Kotecki D.J.: Predicted and measured FN in specifications – A position statement of the experts of IIW Commission IX, Doc. IIW-1420, Welding in the World, 1999, vol. 43, no. 2, pp. 8-10.

[52] Iamboliev T., Katayama S. and Matsunawa A.: Interpretation of phase formation in austenitic stainless steel welds, Welding Journal, 2003, no. 12, pp. 337s-347s.

[53] Elmer J.W., Allen S.M. and Eagar T.W.: Microstructural development during solidification of stainless steel alloys, Metallurgical Transactions A., 1989, vol. 20A, pp. 2117-2131.

[54] Suutala N. Effect of Solidification Conditions on the Solidification Mode in Austenitic Stainless Steels. Metallurgical Transactions A. 1983, vol. 14A, no. 2, pp. 191-197.

[55] Elmer J.W., Allen S.M. and Eagar T.W. The influence of cooling rate on the ferrite content of stainless steel alloys, Proceedings of the 2nd International Conference on Trends in Welding Research, Gatlinburg, 14-18 May 1989, Tennessee: ASM International, 1989, pp. 165-170.

[56] Anderson T.D., Perricone M.J., DuPont J.N. and Marder A.R.: The influence of molybdenum on stainless steel weld microstructures, Welding Journal, 2007, vol. 86, no. 9, pp. 281s-292s.

[57] Inoue H., Koseki T., Ohkita S. and Tanaka T.: Effect of solidification on subsequent ferrite-to-austenite massive transformation in an austenitic stainless steel weld metal, ISIJ International, 1995, vol. 35, no. 10, pp. 1248-1257.

[58] Lippold J.C. and Kotecki D.J. Welding metallurgy and weldability of stainless steels, New Jersey: Wiley-Interscience, 2005, ISBN 0-471-47379-0.

[59] Nakao R., Fukumoto S., Fuji M. and Takeuchi H.: Evaporation of Alloying Elements and Behavior of Degassing Reactions of High Chromium Steel in Electron Beam Melting. ISIJ International. 1992, vol. 32, no. 5, pp. 685-692.

[60] Block-Bolten, A. and Eagar T.W.: Metal vaporization from weld pools, Metallurgical Transactions B, 1984, vol. 15B, pp. 461-469.

[61] Jenkins N.T., Mendez P.F. and Eagar T.W.: Effect of Arc welding electrode temperature on vapor and fume composition, ASM International, Trends in Welding Research Conference, Ohio, 2005, 6 pages.

[62] Jenkins N.T and Eagar T.W.: Chemical analysis of welding fume particles, Welding Journal, 2005, vol. 84, no. 6, pp. 87s-93s.

Appendix 1

Calculated samples series [Cr_{eq}+Ni_{eq}] = 40 %

Cr_{eq}/Ni_{eq}	$Cr_{eq}+Ni_{eq}$ [%]	ER310		ER312			ER70S-6		Sample weight [g]
		[%]	[g]	[%]	[g]		[%]	[g]	
1.22	40.49	61.97	30.99	20.20	10.10	(a)	17.83	8.92	50.01
1.24	40.52	60.41	30.20	22.00	11.00	(a)	17.59	8.79	49.99
1.26	40.53	58.71	29.36	23.98	11.99	(a)	17.31	8.66	50.01
1.28	40.58	57.01	28.50	26.01	13.00	(a)	16.98	8.49	49.99
1.30	40.04	55.70	27.85	26.70	13.35	(b)	17.60	8.80	50.00
1.31	40.58	54.01	26.99	29.40	14.69	(a)	16.59	8.29	49.97
1.32	40.58	52.59	26.29	30.99	15.49	(a)	16.42	8.21	49.99
1.34	40.62	51.00	25.50	32.90	16.45	(a)	16.10	8.05	50.00
1.37	40.65	49.02	24.50	35.19	17.59	(a)	15.79	7.89	49.98
1.38	40.61	47.70	23.85	36.60	18.30	(a)	15.70	7.85	50.00
1.40	40.01	48.00	24.00	35.50	17.75	(b)	16.50	8.25	50.00
1.42	40.67	44.79	22.39	40.03	20.01	(a)	15.18	7.59	49.99
1.43	40.68	43.50	21.75	41.50	20.75	(a)	15.00	7.50	50.00
1.44	40.66	42.50	21.25	42.60	21.30	(a)	14.90	7.45	50.00
1.46	40.67	41.10	20.56	44.18	22.10	(a)	14.72	7.36	50.02
1.48	40.71	39.50	19.74	46.10	23.04	(a)	14.40	7.20	49.98
1.50	40.02	41.00	20.50	43.60	21.80	(b)	15.40	7.70	50.00
1.52	40.71	36.49	18.25	49.49	24.75	(a)	14.02	7.01	50.01
1.54	40.00	38.00	19.00	47.00	23.50	(b)	15.00	7.50	50.00
1.55	40.01	37.50	18.75	47.60	23.80	(b)	14.90	7.45	50.00
1.57	40.03	36.50	18.25	48.80	24.40	(b)	14.70	7.35	50.00
1.59	40.02	35.00	17.50	50.50	25.25	(b)	14.50	7.25	50.00
1.60	40.04	34.60	17.30	51.00	25.50	(b)	14.40	7.20	50.00
1.62	40.00	33.30	16.65	52.40	26.20	(b)	14.30	7.15	50.00
1.64	40.81	28.20	14.10	59.10	29.55	(a)	12.70	6.35	50.00
1.65	40.77	27.00	13.51	60.38	30.21	(a)	12.62	6.31	50.03
1.67	40.80	25.99	13.00	61.59	30.80	(a)	12.42	6.21	50.01
1.68	40.81	25.03	12.51	62.69	31.34	(a)	12.28	6.14	49.99
1.70	40.82	23.99	12.00	63.89	31.95	(a)	12.12	6.06	50.01
1.72	40.81	22.99	11.50	64.99	32.50	(a)	12.02	6.01	50.01
1.73	40.02	26.40	13.20	60.40	30.20	(b)	13.20	6.60	50.00
1.75	40.02	25.10	12.55	61.90	30.95	(b)	13.00	6.50	50.00
1.76	40.00	24.80	12.40	62.20	31.10	(b)	13.00	6.50	50.00
1.78	40.00	23.50	11.75	63.70	31.85	(b)	12.80	6.40	50.00
1.79	40.01	23.00	11.50	64.30	32.15	(b)	12.70	6.35	50.00
1.81	40.00	22.10	11.05	65.30	32.65	(b)	12.60	6.30	50.00
1.83	40.01	21.00	10.50	66.60	33.30	(b)	12.40	6.20	50.00
1.85	40.03	20.00	10.00	67.80	33.90	(b)	12.20	6.10	50.00
1.87	40.00	18.90	9.45	69.00	34.50	(b)	12.10	6.05	50.00
1.89	40.02	17.90	8.95	70.20	35.10	(b)	11.90	5.95	50.00
1.91	40.00	16.90	8.45	71.30	35.65	(b)	11.80	5.90	50.00
1.93	40.02	15.90	7.95	72.50	36.25	(b)	11.60	5.80	50.00
1.95	40.02	14.50	7.25	74.10	37.05	(b)	11.40	5.70	50.00
1.97	40.44	14.00	7.00	75.70	37.85	(b)	10.30	5.15	50.00
2.00	40.02	12.00	6.00	77.00	38.50	(b)	11.00	5.50	50.00

(a) Lot WO14634 and (b) lot WO11381. Different lots of ER312 wire.

Appendix 2

Calculated samples series [Cr_{eq}+Ni_{eq}] = 30 %

Cr_{eq}/Ni_{eq}	Cr_{eq}+Ni_{eq} [%]	310S94		312S94			ER70S-6		Sample weight [g]
		[%]	[g]	[%]	[g]		[%]	[g]	
1.22	30.34	41.71	20.86	19.18	9.59	(a)	39.11	19.56	50.01
1.24	30.35	40.20	20.10	20.90	10.45	(a)	38.90	19.45	50.00
1.26	30.38	39.09	19.55	22.22	11.11	(a)	38.69	19.35	50.01
1.28	30.37	37.49	18.74	24.00	12.00	(a)	38.51	19.25	49.99
1.30	30.01	38.00	19.00	23.00	11.50	(b)	39.00	19.50	50.00
1.31	30.39	35.69	17.85	26.10	13.05	(a)	38.21	19.11	50.01
1.33	30.40	34.29	17.14	27.70	13.85	(a)	38.01	19.00	49.99
1.35	30.42	33.01	16.51	29.19	14.60	(a)	37.80	18.91	50.02
1.37	30.41	32.01	16.01	30.31	15.16	(a)	37.68	18.85	50.02
1.38	30.40	31.19	15.60	31.19	15.60	(a)	37.62	18.81	50.01
1.40	30.04	31.90	15.95	30.10	15.05	(b)	38.00	19.00	50.00
1.41	30.46	29.11	14.55	33.69	16.84	(a)	37.20	18.59	49.98
1.43	30.44	27.92	13.96	34.98	17.49	(a)	37.10	18.55	50.00
1.45	30.48	27.12	13.56	35.99	18.00	(a)	36.89	18.45	50.01
1.47	30.47	26.00	13.00	37.22	18.61	(a)	36.78	18.39	50.00
1.48	30.49	25.02	12.51	38.39	19.19	(a)	36.59	18.29	49.99
1.50	30.00	26.70	13.35	36.00	18.00	(b)	37.30	18.65	50.00
1.53	30.47	22.50	11.25	41.19	20.59	(a)	36.31	18.15	49.99
1.55	30.00	24.00	12.00	39.10	19.55	(b)	36.90	18.45	50.00
1.57	30.00	22.80	11.40	40.50	20.25	(b)	36.70	18.35	50.00
1.59	30.04	22.10	11.05	41.40	20.70	(b)	36.50	18.25	50.00
1.61	30.23	21.20	10.60	42.90	21.45	(b)	35.90	17.95	50.00
1.63	30.25	20.20	10.10	44.10	22.05	(b)	35.70	17.85	50.00
1.65	30.23	19.19	9.60	45.20	22.61	(b)	35.61	17.81	50.02
1.68	30.25	18.19	9.10	46.40	23.21	(b)	35.41	17.71	50.02
1.70	30.24	17.30	8.65	47.40	23.70	(b)	35.30	17.65	50.00
1.71	30.24	16.80	8.40	47.99	24.00	(b)	35.21	17.61	50.01
1.73	30.01	15.70	7.85	48.70	24.35	(b)	35.60	17.80	50.00
1.75	30.03	14.70	7.35	49.90	24.95	(b)	35.40	17.70	50.00
1.77	30.02	13.90	6.95	50.80	25.40	(b)	35.30	17.65	50.00
1.79	30.01	13.00	6.50	51.80	25.90	(b)	35.20	17.60	50.00
1.81	30.01	12.30	6.15	52.60	26.30	(b)	35.10	17.55	50.00
1.83	30.25	11.60	5.80	54.00	27.00	(b)	34.40	17.20	50.00
1.85	30.25	10.90	5.45	54.80	27.40	(b)	34.30	17.15	50.00
1.87	30.28	10.00	5.00	55.90	27.95	(b)	34.10	17.05	50.00
1.88	30.25	9.50	4.75	56.40	28.20	(b)	34.10	17.05	50.00
1.90	30.28	8.70	4.35	57.40	28.70	(b)	33.90	16.95	50.00
1.92	30.27	7.90	3.95	58.30	29.15	(b)	33.80	16.90	50.00
1.95	30.25	7.00	3.50	59.29	29.65	(b)	33.71	16.86	50.01
1.96	30.26	6.40	3.20	60.00	30.00	(b)	33.60	16.80	50.00
1.98	30.26	5.80	2.90	60.70	30.35	(b)	33.50	16.75	50.00
2.00	30.00	5.00	2.50	61.00	30.50	(b)	34.00	17.00	50.00

(a) Lot WO14634 and (b) Lot WO11381. Different lots of ER312 wire.

Appendix 3

Calculated chemical composition for [Cr_{eq}+Ni_{eq}] = 40 % series [wt. %]

Sample	C	Mn	Si	S	P	Cr	Ni	N	O	Mo	Cr_{eq}/ Ni_{eq}
A18	0.102	1.68	0.44	0.0032	0.014	22.19	14.65	0.058	0.009	0.06	1.22
A19	0.102	1.69	0.44	0.0032	0.014	22.33	14.49	0.060	0.009	0.06	1.24
A20	0.102	1.69	0.44	0.0031	0.015	22.49	14.32	0.062	0.009	0.06	1.26
A21	0.102	1.69	0.44	0.0031	0.015	22.66	14.15	0.064	0.009	0.06	1.28
A22R	0.102	1.68	0.41	0.0031	0.015	22.55	13.94	0.048	0.009	0.09	1.30
A23	0.102	1.70	0.44	0.0030	0.015	22.91	13.85	0.068	0.009	0.07	1.31
A24	0.102	1.70	0.44	0.0030	0.015	23.03	13.70	0.070	0.009	0.07	1.32
A25	0.102	1.71	0.44	0.0029	0.015	23.20	13.54	0.072	0.009	0.07	1.34
A26	0.102	1.71	0.44	0.0029	0.015	23.38	13.35	0.075	0.009	0.07	1.37
A27	0.102	1.71	0.44	0.0028	0.016	23.46	13.20	0.076	0.009	0.07	1.38
A28R	0.102	1.69	0.41	0.0029	0.016	23.22	13.15	0.052	0.009	0.10	1.40
A29	0.102	1.72	0.44	0.0027	0.016	23.75	12.91	0.080	0.009	0.07	1.42
A30	0.102	1.72	0.44	0.0027	0.016	23.86	12.78	0.082	0.009	0.07	1.43
A31	0.102	1.72	0.44	0.0027	0.016	23.93	12.68	0.083	0.009	0.07	1.44
A32	0.102	1.73	0.44	0.0027	0.016	24.05	12.53	0.085	0.009	0.07	1.46
A33	0.102	1.73	0.44	0.0026	0.016	24.21	12.38	0.087	0.009	0.08	1.48
A34R	0.102	1.70	0.40	0.0027	0.017	23.86	12.45	0.056	0.009	0.11	1.50
A35	0.102	1.74	0.44	0.0025	0.017	24.46	12.07	0.091	0.009	0.08	1.52
A54R	0.102	1.71	0.40	0.0026	0.017	24.12	12.14	0.058	0.009	0.12	1.54
A55R	0.102	1.71	0.40	0.0026	0.017	24.17	12.09	0.058	0.009	0.12	1.55
A56R	0.102	1.71	0.39	0.0025	0.018	24.28	11.99	0.059	0.009	0.12	1.57
A57R	0.102	1.71	0.39	0.0025	0.018	24.40	11.84	0.059	0.009	0.12	1.59
A58R	0.102	1.71	0.39	0.0025	0.018	24.45	11.80	0.060	0.009	0.12	1.60
A59R	0.102	1.71	0.39	0.0025	0.018	24.54	11.66	0.060	0.009	0.13	1.62
A60	0.102	1.75	0.44	0.0023	0.017	25.23	11.23	0.102	0.009	0.08	1.64
A61	0.102	1.76	0.44	0.0023	0.018	25.30	11.10	0.103	0.009	0.08	1.65
A62	0.102	1.76	0.44	0.0022	0.018	25.41	11.01	0.105	0.009	0.08	1.67
A63	0.102	1.76	0.44	0.0022	0.018	25.49	10.91	0.106	0.009	0.08	1.68
A64	0.102	1.76	0.44	0.0022	0.018	25.59	10.80	0.107	0.010	0.09	1.70
A65	0.102	1.77	0.44	0.0021	0.018	25.66	10.70	0.108	0.010	0.09	1.72
A66R	0.102	1.72	0.38	0.0023	0.019	25.18	10.96	0.064	0.009	0.14	1.73
A67R	0.102	1.73	0.38	0.0022	0.019	25.30	10.83	0.065	0.009	0.14	1.75
A68R	0.102	1.73	0.38	0.0022	0.019	25.31	10.80	0.065	0.010	0.14	1.76
A69R	0.102	1.73	0.38	0.0022	0.019	25.43	10.66	0.066	0.010	0.14	1.78
A70R	0.102	1.73	0.38	0.0022	0.019	25.48	10.62	0.066	0.010	0.14	1.79
A71R	0.102	1.73	0.38	0.0021	0.019	25.55	10.52	0.067	0.010	0.14	1.81
A711	0.102	1.73	0.38	0.0021	0.019	25.66	10.41	0.067	0.010	0.15	1.83
A712	0.102	1.73	0.38	0.0021	0.020	25.76	10.32	0.068	0.010	0.15	1.85
A713	0.102	1.74	0.38	0.0020	0.020	25.84	10.20	0.069	0.010	0.15	1.87
A714	0.102	1.74	0.37	0.0020	0.020	25.95	10.10	0.069	0.010	0.15	1.89
A715	0.102	1.74	0.37	0.0020	0.020	26.02	9.99	0.070	0.010	0.15	1.91
A716	0.102	1.74	0.37	0.0019	0.020	26.13	9.90	0.070	0.010	0.16	1.93
A72R	0.102	1.74	0.37	0.0019	0.020	26.25	9.75	0.071	0.010	0.16	1.95
A73	0.102	1.75	0.37	0.0018	0.020	26.61	9.80	0.072	0.010	0.16	1.97
A731	0.102	1.75	0.37	0.0018	0.020	26.48	9.50	0.072	0.010	0.16	2.00

Appendix 4

Calculated chemical composition for [Cr_{eq}+Ni_{eq}] = 30 % series [wt. %]

Sample	C	Mn	Si	S	P	Cr	Ni	N	O	Mo	Cr_{eq}/ Ni_{eq}
A36	0.095	1.62	0.54	0.0052	0.014	16.63	10.37	0.048	0.009	0.05	1.22
A37	0.095	1.63	0.54	0.0052	0.014	16.76	10.22	0.050	0.009	0.05	1.24
A38	0.095	1.63	0.54	0.0052	0.014	16.88	10.11	0.052	0.009	0.05	1.26
A39	0.095	1.63	0.54	0.0051	0.014	17.00	9.94	0.054	0.009	0.05	1.28
A40R	0.095	1.62	0.52	0.0052	0.015	16.84	9.95	0.038	0.009	0.07	1.30
A41	0.095	1.64	0.54	0.0051	0.014	17.17	9.76	0.056	0.009	0.05	1.31
A42	0.095	1.64	0.54	0.0050	0.014	17.29	9.62	0.058	0.009	0.05	1.33
A43	0.095	1.64	0.54	0.0050	0.015	17.41	9.49	0.059	0.009	0.05	1.35
A44	0.095	1.64	0.54	0.0050	0.015	17.49	9.39	0.061	0.009	0.05	1.37
A45	0.095	1.65	0.54	0.0050	0.015	17.55	9.30	0.062	0.009	0.06	1.38
A46R	0.095	1.63	0.51	0.0050	0.015	17.41	9.34	0.041	0.009	0.08	1.40
A47	0.095	1.65	0.54	0.0049	0.015	17.77	9.10	0.065	0.009	0.06	1.41
A48	0.095	1.65	0.54	0.0049	0.015	17.85	8.97	0.066	0.009	0.06	1.43
A49	0.095	1.65	0.54	0.0048	0.015	17.95	8.90	0.067	0.009	0.06	1.45
A50	0.095	1.66	0.54	0.0048	0.015	18.03	8.78	0.068	0.009	0.06	1.47
A51	0.095	1.66	0.54	0.0048	0.015	18.13	8.69	0.070	0.009	0.06	1.48
A52R	0.095	1.64	0.50	0.0048	0.016	17.86	8.80	0.044	0.009	0.09	1.50
A53	0.095	1.66	0.54	0.0047	0.016	18.33	8.42	0.073	0.010	0.06	1.53
A531	0.095	1.64	0.50	0.0048	0.016	18.10	8.53	0.045	0.010	0.09	1.55
A532	0.095	1.64	0.50	0.0047	0.016	18.21	8.41	0.046	0.010	0.10	1.57
A533	0.095	1.64	0.50	0.0047	0.016	18.30	8.34	0.047	0.010	0.10	1.59
A74	0.095	1.65	0.50	0.0046	0.017	18.52	8.30	0.048	0.010	0.10	1.61
A75	0.095	1.65	0.49	0.0046	0.017	18.63	8.20	0.048	0.010	0.10	1.63
A76	0.095	1.65	0.49	0.0046	0.017	18.70	8.09	0.049	0.010	0.10	1.65
A77	0.095	1.65	0.49	0.0045	0.017	18.81	7.99	0.049	0.010	0.11	1.68
A78	0.095	1.65	0.49	0.0045	0.017	18.88	7.90	0.050	0.010	0.11	1.70
A79	0.095	1.65	0.49	0.0045	0.017	18.93	7.85	0.050	0.010	0.11	1.71
A80R	0.095	1.65	0.49	0.0045	0.017	18.86	7.69	0.050	0.010	0.11	1.73
A81R	0.095	1.65	0.49	0.0045	0.017	18.96	7.59	0.051	0.010	0.11	1.75
A82R	0.095	1.66	0.49	0.0045	0.017	19.03	7.51	0.051	0.010	0.11	1.77
A83R	0.095	1.66	0.49	0.0044	0.017	19.10	7.41	0.052	0.010	0.11	1.79
A84R	0.095	1.66	0.49	0.0044	0.018	19.16	7.34	0.052	0.010	0.11	1.81
A85	0.095	1.66	0.49	0.0043	0.018	19.40	7.33	0.053	0.010	0.12	1.83
A86	0.095	1.66	0.48	0.0043	0.018	19.47	7.25	0.053	0.010	0.12	1.85
A87	0.095	1.66	0.48	0.0043	0.018	19.57	7.17	0.054	0.010	0.12	1.87
A88	0.095	1.66	0.48	0.0043	0.018	19.59	7.11	0.054	0.010	0.12	1.88
A89	0.095	1.67	0.48	0.0042	0.018	19.68	7.04	0.055	0.010	0.12	1.90
A90	0.095	1.67	0.48	0.0042	0.018	19.75	6.95	0.055	0.010	0.12	1.92
A91	0.095	1.67	0.48	0.0042	0.018	19.82	6.86	0.056	0.010	0.12	1.95
A92	0.095	1.67	0.48	0.0042	0.018	19.88	6.80	0.056	0.010	0.13	1.96
A93	0.095	1.67	0.48	0.0042	0.018	19.93	6.74	0.056	0.010	0.13	1.98
A94	0.095	1.67	0.48	0.0042	0.018	19.82	6.60	0.056	0.010	0.13	2.00

Appendix 5

Experimental chemical composition of [Cr_{eq}+Ni_{eq}] = 40 % series (OES determination) [wt. %]

Sample	C	Mn	Si	S	P	Cr	Ni	N**	O**	Mo
A18	0.0776	1.593	0.4853	0.0080	0.0160	21.97	14.85	0.1748	0.0231	0.0755
A19	0.0805	1.607	0.4810	0.0055	0.0138	22.16	14.66	0.0629	0.0016	0.0769
A20	0.0863	1.600	0.4871	0.0051	0.0140	22.16	14.56	0.0522	0.0364	0.0783
A21	0.0945	1.616	0.4891	0.0050	0.0138	22.23	14.39	0.0496	0.0377	0.0790
A22R	0.0871	1.598	0.4946	0.0051	0.0169	22.60	14.16	0.2543	>0.0660	0.1030
A23	0.1005	1.622	0.5070	0.0044	0.0136	22.46	14.17	0.0537	0.0295	0.0812
A24	0.0857	1.605	0.4919	0.0052	0.0145	22.63	13.92	0.0517	0.0136	0.0818
A25	0.0830	1.624	0.4907	0.0047	0.0135	22.79	13.76	0.1461	0.0278	0.0827
A26	0.0968	1.612	0.5080	0.0047	0.0142	22.97	13.62	0.0515	0.0355	0.0847
A27	0.0820	1.639	0.4879	0.0061	0.0155	23.16	13.30	0.1050	0.0191	0.0837
A28R	0.0881	1.626	0.4841	0.0046	0.0170	23.27	13.37	0.2219	>0.0660	0.1129
A29	0.0865	1.647	0.4923	0.0055	0.0150	23.24	13.07	0.1248	0.0205	0.0852
A30	0.0823	1.642	0.4778	0.0058	0.0158	23.65	12.84	0.1143	0.0178	0.0860
A31	0.0876	1.652	0.4849	0.0053	0.0154	23.63	12.80	0.0812	0.0057	0.0881
A32	0.0862	1.658	0.4850	0.0054	0.0149	23.81	12.60	0.1342	0.0248	0.0875
A33	0.0911	1.661	0.4980	0.0042	0.0147	23.83	12.55	0.0607	0.0391	0.0900
A34R	0.0861	1.644	0.4755	0.0043	0.0182	23.77	12.75	0.1244	0.0630	0.1239
A35	0.0909	1.661	0.5000	0.0043	0.0151	24.06	12.26	0.0736	0.0209	0.0921
A54R	0.0874	1.652	0.4662	0.0039	0.0179	24.15	12.30	0.0410	0.0129	0.1294
A55R	0.0905	1.620	0.4165	0.0055	0.0192	24.06	12.01	>0.4800	0.0581	0.1291
A56R	0.0884	1.632	0.4241	0.0054	0.0201	24.19	12.15	0.1445	0.0068	0.1312
A57R	0.0845	1.608	0.4129	0.0054	0.0191	24.26	11.68	>0.4800	0.0617	0.1318
A58R	0.0863	1.630	0.4157	0.0051	0.0197	24.33	11.86	0.3562	0.0421	0.1336
A59R	0.0925	1.642	0.4222	0.0050	0.0197	24.41	11.81	0.2328	0.0294	0.1352
A60	0.1233	1.726	0.4705	0.0043	0.0157	24.94	11.22	0.0802	0.0280	0.0952
A61	0.1411	1.721	0.4698	0.0034	0.0149	25.41	11.11	0.0737	0.0165	0.0937
A62	0.1429	1.713	0.4751	0.0034	0.0154	25.30	11.02	0.0761	0.0329	0.0962
A63	0.1111	1.695	0.4533	0.0049	0.0172	25.73	10.70	0.1625	0.0199	0.0962
A64	0.0826	1.708	0.4741	0.0048	0.0173	25.70	10.79	0.1232	0.0142	0.0971
A65	0.0836	1.703	0.4711	0.0056	0.0180	25.83	10.64	0.1151	–	0.0969
A66R	0.0897	1.644	0.4145	0.0048	0.0208	24.98	11.13	0.2867	0.0331	0.1473
A67R	0.0894	1.642	0.4124	0.0051	0.0210	25.19	10.92	0.3836	0.0387	0.1497
A68R	0.0893	1.603	0.4125	0.0053	0.0216	25.09	10.93	0.2733	0.0135	0.1504
A69R	0.0937	1.654	0.4195	0.0043	0.0202	25.17	10.82	0.1072	0.0047	0.1524
A70R	0.0866	1.630	0.4063	0.0049	0.0212	25.29	10.66	0.4100	0.0443	0.1530
A71R	0.0910	1.653	0.4127	0.0049	0.0219	25.25	10.67	0.1212	<0.0010	0.1530
A711	0.0925	1.657	0.4167	0.0046	0.0216	25.33	10.56	0.1719	0.0193	0.1548
A712	0.0942	1.666	0.4187	0.0047	0.0221	25.36	10.55	0.1282	0.0078	0.1579
A713	0.0900	1.660	0.4052	0.0047	0.0219	25.56	10.29	>0.4800	0.0595	0.1581
A714	0.0921	1.657	0.4125	0.0049	0.0221	25.43	10.17	0.2909	0.0357	0.1595
A715	0.0889	1.656	0.4024	0.0047	0.0214	25.65	10.08	0.3074	0.0276	0.1609
A716	0.0915	1.658	0.4017	0.0049	0.0217	25.45	9.77	0.3370	0.0303	0.1616
A72R	0.0897	1.656	0.4017	0.0045	0.0224	26.00	9.79	0.1927	0.0128	0.1671
A73	0.0828	1.688	0.3974	0.0033	0.0206	26.72	9.81	0.0940	0.0048	0.1698
A731	0.0923	1.651	0.3936	0.0043	0.0221	26.27	9.46	0.3659	0.0418	0.1701

*** Abnormal values. See text for explanation.*

Appendix 6

Experimental chemical composition of [Cr_{eq}+Ni_{eq}] = 30 % series (OES determination) [wt. %]

Sample	C	Mn	Si	S	P	Cr	Ni	N**	O**	Mo
A36	0.0831	1.579	0.580	0.0094	0.0148	16.50	10.55	0.0714	0.0465	0.0598
A37	0.0844	1.589	0.576	0.0080	0.0133	16.71	10.38	0.1498	0.0596	0.0597
A38	0.0881	1.594	0.585	0.0075	0.0129	16.73	10.31	0.1068	0.0615	0.0620
A39	0.0866	1.598	0.584	0.0080	0.0142	16.95	10.15	0.1098	0.0661	0.0623
A40R	0.0933	1.563	0.615	0.0078	0.0160	16.67	10.25	0.1359	>0.2400	0.0845
A41	0.0945	1.594	0.590	0.0060	0.0122	16.98	10.05	0.0411	0.0479	0.0635
A42	0.0884	1.607	0.579	0.0073	0.0131	17.12	9.80	0.1147	0.0551	0.0714
A43	0.0816	1.611	0.549	0.0052	0.0110	17.33	9.57	0.0772	0.0100	0.0603
A44	0.0878	1.586	0.560	0.0059	0.0123	17.36	9.43	0.0639	0.0020	0.0616
A45	0.0875	1.572	0.558	0.0068	0.0132	17.46	9.34	0.1161	<0.0010	0.0624
A46R	0.0891	1.585	0.590	0.0061	0.0158	17.35	9.60	0.2974	0.1623	0.0923
A47	0.0893	1.597	0.560	0.0057	0.0124	17.71	9.16	0.1289	0.0024	0.0649
A48	0.0783	1.598	0.561	0.0057	0.0128	17.73	9.06	0.0644	<0.0010	0.0635
A49	0.0805	1.592	0.552	0.0063	0.0138	17.91	8.89	0.0856	<0.0010	0.0641
A50	0.0855	1.592	0.562	0.0065	0.0133	17.95	8.77	0.2242	0.0072	0.0652
A51	0.0821	1.598	0.553	0.0064	0.0141	18.07	8.65	0.0910	<0.0010	0.0650
A52R	0.0872	1.602	0.596	0.0054	0.0161	17.78	9.19	0.0928	0.0925	0.1005
A53	0.0838	1.602	0.561	0.0061	0.0140	18.23	8.49	0.0581	<0.0010	0.0669
A531	0.0789	1.607	0.586	0.0048	0.0156	18.31	8.80	0.0531	0.0518	0.1034
A532	0.0850	1.616	0.588	0.0054	0.0158	18.33	8.61	0.1612	0.0638	0.1053
A533	0.0843	1.609	0.583	0.0050	0.0167	18.54	8.65	0.0694	0.0264	0.1070
A74	0.1393	1.613	0.529	0.0060	0.0165	18.93	8.48	0.0594	0.0346	0.1116
A75	0.0757	1.613	0.510	0.0065	0.0175	19.15	8.27	0.0786	0.0108	0.1107
A76	0.0786	1.614	0.508	0.0058	0.0162	19.19	8.11	0.0571	0.0061	0.1126
A77	0.0822	1.612	0.523	0.0063	0.0162	19.30	8.17	0.0811	0.0258	0.1166
A78	0.0740	1.617	0.507	0.0065	0.0174	19.49	7.98	0.1013	0.0225	0.1153
A79	0.0844	1.618	0.507	0.0035	0.0137	19.44	7.93	0.1241	0.0298	0.1173
A80R	0.0857	1.615	0.525	0.0065	0.0188	18.83	7.97	0.1519	0.0279	0.1157
A81R	0.0813	1.596	0.514	0.0062	0.0183	18.97	7.82	0.1005	0.0134	0.1171
A82R	0.0889	1.606	0.531	0.0064	0.0191	19.16	7.73	0.1620	0.0153	0.1192
A83R	0.0821	1.554	0.526	0.0064	0.0188	19.06	7.75	0.1183	0.0248	0.1207
A84R	0.0867	1.611	0.521	0.0069	0.0197	19.15	7.56	0.2749	0.0318	0.1215
A85	0.0793	1.617	0.515	0.0064	0.0189	19.89	7.51	0.0492	--	0.1252
A86	0.0739	1.612	0.496	0.0065	0.0192	20.00	7.36	0.0997	--	0.1270
A87	0.0743	1.631	0.501	0.0059	0.0184	20.17	7.26	0.1120	--	0.1277
A88	0.0720	1.619	0.511	0.0061	0.0185	20.05	7.30	0.0737	--	0.1286
A89	0.0728	1.622	0.495	0.0057	0.0186	20.33	7.07	0.0884	--	0.1305
A90	0.0791	1.642	0.503	0.0051	0.0176	20.21	7.14	0.0763	--	0.1314
A91	0.0795	1.619	0.504	0.0060	0.0194	20.35	6.92	0.0628	--	0.1345
A92	0.0833	1.633	0.506	0.0059	0.0193	20.37	6.95	0.0661	--	0.1350
A93	0.0842	1.623	0.493	0.0042	0.0166	20.47	6.83	0.0690	--	0.1379
A94	0.0897	1.611	0.512	0.0059	0.0200	19.86	6.76	0.1572	0.0118	0.1342

*** Abnormal values. See text for explanation.*